PL-TR-96-2287

INCOHERENT-SCATTER VERIFICATION OF DMSP OBSERVATIONS

Jeffrey P. Thayer

SRI International
333 Ravenswood Avenue
Menlo Park, CA 94025-3493

November 1996

Final Report
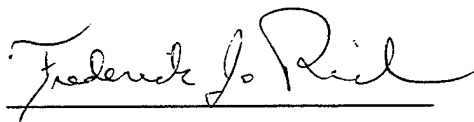September 1994-August 1996

PHILLIPS LABORATORY
Directorate of Geophysics
AIR FORCE MATERIEL COMMAND
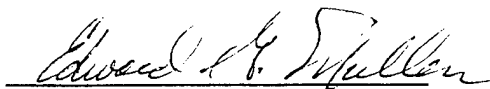**HANSCOM AFB, MA 01731-3010**

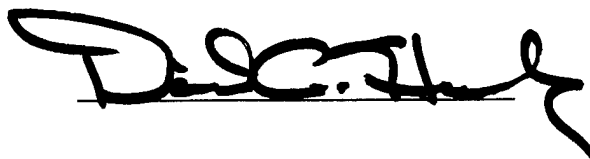19970630 013

DTIC QUALITY INSPECTED 1

"This Technical report has been reviewed and is approved for publication"

FREDERICK RICH
Contract Manager

EDWARD G. MULLEN
Branch Chief

DAVID A. HARDY
Division Director

This report has been reviewed by the ESC Public Affairs Office (PA) and is releasable to the National Technical Information Service (NTIS).

Qualified requestors may obtain additional copies from the Defense Technical Information Center (DTIC). All others should apply to the National Technical Information Service (NTIS).

If your address has changed, or if you wish to be removed from the mailing list, or if the addressee is no longer employed by your organization, please notify PL/TBS, 29 Randolph Road, Hanscom AFB, MA 01731-3010. This will assist us in maintaining a current mailing list.

Do not return copies of this report unless contractual obligations or notices on a specific document requires that it be returned.

REPORT DOCUMENTATION PAGE

Public reporting burden for this collection of information is estimated to average 1 hour per response, including the time for reviewing instructions, searching existing data sources, gathering and maintaining the data needed, and completing and reviewing the collection of information. Send comments regarding this burden estimate or any other aspect of this collection of information, including suggestions for reducing this burden, to Washington Headquarters Services, Directorate for Information Operations and Reports, 1215 Jefferson Davis Highway, Suite 1204, Arlington, VA 22202-4302, and to the Office of Management and Budget, Paperwork Reduction Project (0704-0188), Washington, DC 20503.

1. AGENCY USE ONLY (Leave Blank)	2. REPORT DATE	3. REPORT TYPE AND DATES COVERED
	November 1996	Final—September 1994 through August 1996

4. TITLE AND SUBTITLE

Incoherent-Scatter Verification of DMSP Observations

6. AUTHORS

Jeffrey P. Thayer

5. FUNDING NUMBERS

PE 35160F

PR 1924 TA GB WU MC

F19628-94-C-0100

7. PERFORMING ORGANIZATION NAME(S) AND ADDRESS(ES)

SRI International
333 Ravenswood Avenue
Menlo Park, CA 94025-3493

8. PERFORMING ORGANIZATION REPORT NUMBER

9. SPONSORING/MONITORING AGENCY NAME(S) AND ADDRESS(ES

Phillips Laboratory
29 Randolph Road
Hanscom AFB. MA 01731-3010
Contract Manager: Frederick Rich/GPSP

10. SPONSORING/MONITORING AGENCY REPORT NUMBER

PL–TR–96–2287

11. SUPPLEMENTARY NOTES

12a. DISTRIBUTION/AVAILABILITY STATEMENT

Approved for public release;

distribution unlimited

12b. DISTRIBUTION CODE

13. ABSTRACT *(Maximum 200 words)*

The transfer of electromagnetic energy to heat, that is, Joule heating, in the ionospheric gas is often the most dominant energy source for the winter polar regions. The Defense Meteorological Satellite Program (DMSP) has demonstrated that the Joule heating rate in the high-latitude ionosphere can be estimated with satellite measurements of the perturbation magnetic field and precipitating particle population. These estimates of the Joule heating rate are subject to a number of assumptions and empirical formalisms that require validation. The NSF incoherent-scatter radar located at Sondrestrom, Greenland, can measure the plasma parameters of interest and is at a latitude well suited for coincident measurements with DMSP. In this report, we summarize the effort made over the 2-year project and provide details of the observational and analysis program. This effort involved a dedicated 9-month observational program, improving radar estimates of Joule heating and conductance for comparison with DMSP, testing assumptions used in the DMSP derivation of the Joule heating rate, comparing DMSP and radar conductance estimates, and establishing a capability for rapid validation of the Joule heating rate for future conjunctions with DMSP satellites.

14. SUBJECT TERMS

high-latitude ionosphere   Joule heating rate   incoherent-scatter radar

15. NUMBER OF PAGES

50

16. PRICE CODE

17. SECURITY CLASSIFICATION OF REPORT	18. SECURITY CLASSIFICATION OF THIS PAGE	19. SECURITY CLASSIFICATION OF ABSTRACT	20. LIMITATION OF ABSTRACT
Unclassified	Unclassified	Unclassified	Unlimited

CONTENTS

LIST OF ILLUSTRATIONS

1 INTRODUCTION

The high-latitude E region is subject to several sources of energy—that is, solar UV/EUV radiation, electromagnetic energy (resulting in Joule heating and mechanical energy transfer), particle precipitation, atmospheric waves and tides, and magnetospheric waves. At times and for specific altitudes within the E region, any of these energy sources, expressed in terms of energy flux (Wm^{-2}), may dominate. Of these, the magnetospheric sources have the most profound effect on the high-latitude E region with, for example, the Joule heating rate and the heating rate due to particle precipitation (each reaching $100\ mWm^{-2}$), far exceeding direct heating by solar EUV energy (1 to $3\ mWm^{-2}$) within the auroral oval [e.g., Banks, 1977]. Although Joule heating and particle heating are closely linked features of the high-latitude E region, their impact on the ion and neutral gas is very different. This is due, in part, to the fact that Joule heating is transferred to heat in the E region over larger regions and more efficiently than precipitating particle energy [e.g., Vickrey et al., 1982]. In addition, the altitude of maximum energy deposition from Joule heating is higher than particle precipitation [Brekke and Rino, 1978].

These energy sources, however, are not completely separable in their contribution to the total heating rate of the E region. The energetics of particle precipitation that enhance the E-region conductances and the coincident location of the enhanced conductances with the converging electric fields will significantly impact the Joule heating rate. This was demonstrated, for example, by Vickrey et al. [1982] who showed that the magnitude of energy input by precipitating particles (maximizing in the morning sector) often has the opposite asymmetry about midnight to that of Joule heating (maximizing in the dusk sector). Solar EUV radiation has an important indirect contribution to the net heating of the high-latitude E region as it is a principal source of E-region ionization and conductivity. Robinson and Vondrak [1984] demonstrated that the conductance produced by solar illumination during solar minimum is comparable to that produced by the diffuse aurora and far exceeds the diffuse aurora during solar maximum conditions. The uniform distribution in conductivity caused by solar illumination and the uncoupled nature of the process to large-scale changes in the electric field can result in the solar illumination indirectly having a major contribution to the heating of the E region.

The Defense Meteorological Satellite Program (DMSP) has demonstrated that the Joule heating rate in the high-latitude ionosphere can be estimated from spacecraft [Rich et al., 1987; 1991]. These estimates of the Joule heating rate are subject to a number of assumptions that require validation. Independent ground observations of the same heating process have, therefore, been employed to test the validity of some of these assumptions. The NSF incoherent-scatter radar located at Sondrestrom, Greenland, can measure the plasma parameters of interest and is at a latitude well-suited for coincident measurements with DMSP. Until recently, the radar facility had its limitations in accounting for the effects of the neutral wind on the Joule heating rate in the E region. However, the recent improvement in altitude resolution and signal statistics in the E region has permitted the Joule heating rate to be more accurately determined by accounting for neutral wind effects. Also, the manner in which the Joule heating rate is now being calculated

1

parallels that of Rich et al. [1987] allowing a more direct means of testing assumptions and comparing results.

This report summarizes the progress made during the project and details the observational and analysis program for conjunctions with the F12 and F13 DMSP satellites and the radar.

2 PROJECT TASKS

Over the course of the project, we completed all of the tasks stated in the original statement of work. The following restates the individual tasks and provides the level of accomplishment.

Task 1: Implement and test the radar operating model designed for DMSP coordination prior to spacecraft launch, and supply sample data to Phillips Laboratory (PL).

Details: Section 4.1

Since the F7 study, the Sondrestrom radar has improved its range resolution to as good as 3 km using an alternating code pulse scheme (see Scientific Report No. 1). This pulse scheme reduces pulse smearing effects significantly and, although limited by statistical noise, yields far superior measurement statistics when compared to multipulse techniques with similar range resolutions. Our emphasis has been the development of an observing mode that provides a direct, and highly accurate, characterization of background plasma density and drift from a sequence of fixed-position measurements for improved estimates of conductance and Joule heating.

Task 2: Establish the criteria for radar coordinated runs based upon satellite geometry and geophysical conditions, and implement procedures to schedule radar observations as frequently as site commitments allow.

Details: Section 4.2

The established criteria described in Section 4.2 typically led to the availability of 5 to 10 orbits per month from which to choose for coordinated observations with the radar. About 12 to 15 hours per month of radar time were dedicated to DMSP experiments. Each experiment was of the order of 1 to 3 hours in duration centered on the time of the pass, resulting in about 4 to 5 passes chosen each month.

Task 3: In conjunction with PL, select optimum algorithms and atmospheric models for use with the satellite and radar computation of Joule heating rate, and adapt the radar software to use those algorithms and the A16B high-resolution radar data.

Details: Section 5

The development of the Joule heating rate calculations from the radar using the new high-resolution radar mode has been described in detail in Scientific Report No. 1. Based on these

calculations, a number of important assumptions used in previous radar calculations and in the DMSP calculations were investigated and are summarized in Section 5.1. Evaluation of pulse smearing on conductance calculations and the impact of this effect on previous studies is described in Section 5.2.

Task 4: Evaluate the photoionization model used by PL using data recently collected at Sondrestrom, including consideration of data confidence intervals, and suggest a short-term photoionization dependence if deemed necessary.

Details: Sections 5.2 and 6

The DMSP estimate of conductance assumes three sources of ionospheric ionization to be important: direct solar UV and EUV radiation, cosmic rays and galactic EUV, and the precipitation of energetic electrons downward along magnetic field lines. The high-resolution radar data make it possible to evaluate accurately the total ionospheric conductance and, under different conditions, attempt to separate the sources so their impact on conductance can be elucidated. In Section 6 we compare directly the DMSP and radar estimates for conductance from six select experiments. Three of these experiments were conducted during sunlit conditions while the other three correspond to twilight and nighttime conditions. The daytime measurements allow us to evaluate how well the photoionization model used by DMSP compares with the measurements. The twilight and nighttime experiments test the DMSP conductance estimates by particle precipitation alone. Also, in Section 5.2 we investigated the improved accuracy of determining the conductance from the high-resolution radar measurements as compared to the 48 km pulse scheme used in the DMSP F7/radar study [Watermann and de la Beaujardiére, 1990].

Task 5: Establish a format for summarizing radar data, and supply those data on a timely basis to PL throughout the period of observations.

We have compiled summary plots of the data that constitute a catalogue of observations for a quick overview of the radar data taken during DMSP passes. This involves analyzing the long-pulse data from elevation scans and dwells to give us an indication of the ionospheric conditions during the DMSP flyby. If the conditions are favorable (i.e., if significant structure is present in the E region), we can then begin to analyze the complete radar data set. The catalogue is in hard copy form and can be accessed through SRI.

Task 6: Perform detailed analysis of selected satellite/radar data sets in order to determine the sensitivity of the Joule heating estimates to a neutral model and other assumptions.

Details: Sections 5.1 and 6

We have completed the detailed radar analysis of the Joule heating rate during times of possibly good DMSP conjunctions. These data as well as other periods of radar-derived Joule heating rates have been used to validate the general assumptions used in the DMSP analysis.

3

These results are presented in Section 5.1. The actual comparisons with the DMSP-derived Joule heating rates have been deferred for future evaluation.

Task 7: Maintain a statistical database of radar-observed Joule heating observations collected over the duration of the project.

Radar-derived Joule heating rates have been collected over the duration of the project for observing periods with favorable conditions (i.e., E-region plasma enhancements). We have also begun to collect other favorable periods that may or may not be during DMSP passes but improve our statistical database of Joule heating measurements. The radar analysis of Joule heating will continue and will provide additional conjunctions for future comparisons.

3 ISR OBSERVING PERIODS AND GEOMAGNETIC CONDITIONS

Thirty-nine radar experiments dedicated to DMSP overpasses have been carried out over the course of this project. Table 1 provides some of the details for each of the experiments. It should be noted that other radar operations, not included in Table 1 but coincident with DMSP flybys, which could benefit the DMSP study, may have occurred during this period.

The experiments in Table 1 consist of a combination of orbits that passed near the magnetic meridian (dusk passes) and orbits that were more aligned in the magnetic east–west direction (pre-noon passes). A hardware problem arose in the high-resolution radar data that contaminated the autocorrelation functions preventing us from determining the necessary high-resolution ion drift velocity, ion and electron temperature, and corrected electron density information from data taken between 26 September 1995 and 29 November 1995. The single pulse data and the high-resolution raw density, uncorrected for temperature, recorded during this period were not affected by this problem and, so, some limited information on the Joule heating rate and conductivity can be determined, if the DMSP passes during this period are of significant interest. Table 2 lists the solar flux and geomagnetic activity indices of 3-hour K_p and the daily A_p. The UT corresponding to the stop time of the experiment was used to determine the current K_p value with the prior 6 hours of K_p included to cover conditions before and during the experiment.

By evaluating the geomagnetic conditions and reviewing the signal conditions of the radar data in the E region, we settled on six experiments to perform detailed analysis of the conductance and Joule heating rates for comparison with DMSP estimates. These experiments and the geomagnetic conditions are shown in Tables 1 and 2. Although 39 experiments were carried out, it was still difficult to find experiments that were satisfactory for comparison.

Table 1. Sondrestrom Radar Operations for Primary DMSP Passes

Day No.	Date	Start UT	Stop UT	Satellite	Azimuth	Antenna File	Remarks
076	950317	2130	2359	f12	n-s	f12p002	comp scan
081	950322	1336	1446	f12	e-w	f12p003	comp scan
089	950330	1319	1430	f12	23	f12p004	
152	950601	0932	1053	f13	32	f1395152	active
155	950604	1910	2012	f13	157	f1395155	
160	950609	2233	2351	f12	158	f1295160	
172	950621	1859	2001	f13	151	f1395172	(World Day)
177	950626	0944	1045	f13	28	f1395177	
177	950626	2217	2332	f12	154	f1295177	
182	950701	1308	1430	f12	22	f1295182	
185	950704	0952	1053	f13	23	f1395185	
197	950716	1854	2008	f13	155	f1395197	active
199	950718	1312	1441	f12	21	f1295199	
202	950721	0947	1048	f13	22	f1395202	active
207	950726	1334	1438	f12	23	f1295207	
211	950730	2241	2347	f12	154	f1295211	active
214	950802	1850	2006	f13	154	f1395214	structured
219	950807	2221	2323	f12	155	f1295219	E_s
236	950824	2250	2333	f12	154	f1295236	too windy
239	950827	1902	2009	f13	155	f1395239	quiet
241	950829	1332	1434	f12	22	f1295241	
244	950901	0948	1050	f13	22	f1395244	
252	950910	2237	2350	f12	154	f1295253	
256	950913	1903	2004	f13	154	f1395256	active
269	950926	0925	1023	f13	22	f1395269	A16 problem
295	951022	2217	2352	f12	n-s	f1295295	A16 problem
303	951030	0752	1100	f13	e-w	DMSPns	A16 problem
337	951203	2133	0101	f12	ns	DMSPns	active
339	951205	1752	2105	f13	ns	DMSPns	quiet
340	951206	1744	2100	f13	ns	DMSPns	
345	951211	2150	0102	f12	ns	DMSPns	
006	960106	2150	0101	f12	ns	DMSPns	
008	960108	1751	2103	f13	ns	DMSPns	
014	960114	2155	2209	f12	ns	DMSPns	too windy
025	960125	1741	2104	f13	ns	DMSPns	
031	960131	2147	0101	f12	ns	DMSPns	active
042	960211	1726	2100	f13	ns	DMSPns	active
048	960217	2133	0105	f12	ns	DMSPns	active
050	960219	1801	2102	f13	ns	DMSPns	

Table 2. Geomagnetic Conditions During DMSP Passes

Date	UT	F10.7 (prior day)	F10.7 (81-day average)	K_p (UT–0 hr)	K_p (UT–3 hr)	K_p (UT–6 hr)	A_p (daily)
950317	2359	83.3	82.6	2.0	2.3	2.7	8.0
950322	1446	89.3	81.8	0.7	0.7	1.0	3.0
950330	1430	80.7	81.1	3.0	1.7	1.3	8.0
950601	1053	70.9	77.6	3.3	3.7	4.0	25.0
950604	2012	76.8	77.6	2.0	2.3	1.7	6.0
950609	2351	86.8	77.9	1.7	1.7	1.7	5.0
950621	2001	74.2	77.4	2.0	2.3	2.3	10.0
950626	1045	73.2	76.8	2.7	3.3	4.0	17.0
950626	2332	73.2	76.8	3.0	3.0	2.3	17.0
950701	1430	80.8	76.1	1.7	2.0	2.7	13.0
950704	1053	80.7	76.2	0.7	1.3	2.3	7.0
950716	2008	76.8	76.4	4.3	6.0	5.3	30.0
950718	1441	74.7	76.3	3.3	2.3	2.0	10.0
950721	1048	72.0	76.0	1.7	1.3	0.7	5.0
950726	1438	72.0	75.7	1.7	1.0	1.3	5.0
950730	2347	72.0	75.7	3.0	1.7	1.7	6.0
950802	2006	74.8	75.5	2.7	2.0	1.3	5.0
950807	2323	77.3	75.3	3.0	3.0	2.0	8.0
950824	2333	75.9	73.8	2.3	2.0	1.7	6.0
950827	2009	78.9	73.6	2.3	1.7	1.3	7.0
950829	1434	83.2	73.6	2.0	3.3	2.3	10.0
950901	1050	77.0	74.0	0.7	0.3	0.7	4.0
950910	2350	69.7	75.4	4.7	3.3	2.3	12.0
950913	2004	69.5	75.5	2.3	3.0	2.7	18.0
950926	1023	74.5	75.3	2.0	1.3	1.7	4.0
951022	2352	80.3	74.5	2.7	3.7	1.7	12.0
951030	1100	72.8	74.6	1.7	0.3	0.0	12.0
951203	0101	71.2	72.1	4.3	2.7	3.3	16.0
951205	2105	70.7	72.0	2.3	1.7	0.7	4.0
951206	2100	71.4	72.0	2.0	1.7	1.7	4.0
951211	0102	71.1	71.7	0.3	0.3	1.0	5.0
960106	0101	79.9	70.8	0.7	1.3	1.3	4.0
960108	2103	79.8	70.8	0.3	1.0	1.0	4.0
960114	2209	66.7	70.7	5.3	3.7	3.3	25.0
960125	2104	70.7	70.7	2.3	2.0	1.0	5.0
960131	0101	74.5	70.7	3.0	2.3	2.3	7.0
960211	2100	68.0	70.6	3.0	3.0	2.7	22.0
960217	0105	69.0	70.0	1.3	1.7	2.0	11.0
960219	2102	68.6	69.9	2.3	2.0	0.3	7.0

4 RADAR APPROACH AND OPERATING MODE

4.1 Approach

Incoherent-scatter radar measurements provide the most comprehensive measurement set for estimating the local current, electric field, and conductivity throughout the E region. Neutral winds are also derivable from the radar measurements but are generally limited to altitudes below about 125 km due to the increasing sensitivity to uncertainties in the collision frequency with height along with a dependency on the orientation of the E field. The explicit calculation of the neutral winds in the E region is not necessary if the Joule heating rate is determined by measuring the current density in the E region, as discussed in Scientific Report No. 1. The radar measurements needed to determine the E-region currents are E-region electron density profiles, E-region ion velocity profiles, and F-region ion velocities.

Coordination with spacecraft overpasses requires the radar to make these plasma measurements as a function of latitude, longitude, and time. Under the F7 program, attempts were made to obtain exact spatial and temporal coincidence with the satellite during its overpass using rapid radar elevation scans. In order to derive the full ion vector from the scan data (the key parameter for Joule heating) required certain assumptions; the conclusions from the reported results [Watermann and de la Beaujardiére, 1990] suggest that these assumptions may not always be valid. In addition, further assumptions, not considered at the time of the F7 study, were imposed to derive the conductivity and ion drift from the scan data. These assumptions concern the effects of radar pulse smearing on the derived parameters, such as electron density and ion velocity. For the F7 study, a 48 km radar pulse (long pulse) was used during the scans to provide adequate signal statistics for the determination of the electron density (used in the conductivity calculation) and ion velocity. However, pulse smearing caused by the 48 km pulse can have a significant impact on how well these parameters are determined irrespective of noise and will have important consequences when determining the Joule heating rate. An example of this effect was shown in Scientific Report No. 1. In addition, the calculation of the Joule heating rate in this manner was only approximate as the neutral winds could not be accounted for in the analysis.

Since the F7 study, the Sondrestrom radar has improved its range resolution to as good as 3 km using an alternating code pulse scheme (see Scientific Report No. 1). This pulse scheme reduces pulse smearing effects significantly and, although limited by statistical noise, yields far superior measurement statistics when compared to multipulse techniques with similar range resolutions. The signal statistics are improved by operating the radar in a fixed position mode and integrating the data for a period of about 1 minute. Further range integration can be achieved in post-processing software. Also, we have improved the Joule heating algorithm by taking advantage of the improved range resolution, so that, neutral wind effects on the Joule heating rate can be included in the study. Therefore, rather than trying to obtain exact temporal coincidence with the satellite pass by performing fast elevation scans with a 48 km pulse and having to deal with the problems discussed above, our emphasis has been the development of an observing

mode that provides a direct, and highly accurate, characterization of background plasma density and drift from a sequence of fixed-position measurements. This choice of approach is limiting in one sense: the sequence of measurements to resolve a vector profile takes about 3 minutes. Inherently, then, there is the assumption that there is some degree of homogeneity and temporal stability within the ionosphere. There will be times when the dynamics of the plasma invalidates these assumptions, but with many opportunities for coincidence, data will also be collected under stable magnetic conditions. In those cases, the plasma density and ion drift can be carefully mapped at high range resolution. In addition, single pulse data, like that used in the F7/radar study, have been recorded simultaneously with the high-resolution data so that comparisons can be made to test the assumptions made in the previous study.

4.2 Operating Mode

Criteria for selecting DMSP passes in conjunction with Sondrestrom radar operations are as follows:

- The E-region footprint of the DMSP pass, mapped along the magnetic field line to 125 km, is within 100 km of the Sondrestrom radar.

- The pass is oriented near the magnetic meridian—that is, perpendicular to the L-shell, to allow for nearly maximum latitudinal extent of the radar measurement. This refers to the ascending node of F12 and F13 orbits. These passes are typically in the dusk to midnight local time sectors.

- The period of observation should be during active times. This is crudely estimated by looking at the past 3 months of daily K_p and projecting the periods of active times to the current month. The quiet times seem to be more reproducible so avoidance of those times may also better our chances of geomagnetic activity during the pass.

These criteria typically led to the availability of 5 to 10 orbits per month from which to choose for coordinated observations with the radar. About 12 to 15 hours per month of radar time were dedicated to DMSP experiments. Each experiment is of 1- to 3-hour duration centered on the time of the pass resulting in about 4 to 5 passes chosen each month.

The transmitter waveform used for all of these experiments was the SA16C waveform. The SA16C waveform consists of a standard uncoded 320 μs single pulse (S) at one frequency and 32 separate pulses (A16C), each with different phase code, on the other frequency. The alternating code yield lags 1 through 15 with a baud length/lag spacing of 20 μs. To obtain the zero lag of the autocorrelation function (ACF) a single 20 μs pulse is transmitted with each of the 32 pulses making up the alternating code scheme. The end result is a set of ACFs from the single pulse waveform at 48 km range resolution and a set of ACFs from the alternating code waveform at 3 km range resolution. The ACFs are analyzed using a nonlinear least squares approach to determine the electron density, electron temperature, ion temperature, ion velocity, collision frequency, and composition. The technique used to fit the measured ACF involves the

computation of a theoretical ACF and an unconstrained optimization procedure to perform numerical minimization based on the Levenberg-Marquardt method for each recorded range gate [Zambre, SRI Internal Report, 1993]. The error bars associated with each of the fitted parameters correspond to confidence intervals at the one-sigma level of 68.26%. The long-pulse data are used for estimates of plasma parameters in the F region while the alternating code data are used for estimates of plasma parameters in the E region.

Two radar antenna modes were used for the DMSP/radar experiments. The first radar mode was a specialized antenna mode designed for DMSP volume studies, described in Quarterly Report 1, which we will call the DMSP mode. This experiment essentially consists of an elevation scan followed by 36 position measurements and concluded with another elevation scan. Figure 1 illustrates schematically an example of a DMSP/radar experiment carried out on 2 August 1995 using the DMSP mode. Figure 1(a) displays the radar azimuth-elevation coverage plot for this day showing the position of the radar during the experiment and also the proximity of the DMSP satellite footprint, mapped along the magnetic field line to 125 km, with respect to the radar measurements. By design, the position measurements are in line with the track of the satellite. The sequence of radar measurements is started so that it is centered, in time, on the overhead passage of the satellite.

Figure 1(b) shows the magnetic latitude coverage at 125 km of the radar and DMSP satellite measurements for the 2 August 1995 experiment and the time interval it takes for the radar and DMSP satellite to cover these latitudes. The overall radar data collection time for each DMSP experiment was approximately 1 hour, while the DMSP pass took approximately 120 seconds to cover magnetic latitudes between 71° and 78°. Therefore, the pattern of fixed positions shown in Figure 1(a) provides good spatial resolution while the temporal resolution shown in Figure 1(b) is limited. From this pattern, a resolved velocity can be derived from a minimum of three fixed-position, line-of-sight Doppler measurements. This mode provides the flexibility to choose the appropriate number of positions to resolve the vector based on the conditions at the time of the measurement. Each fixed position measurement in the sequence also provides a measurement of the plasma at all altitudes in the E- and F-region ionosphere. The dense sampling of the ionosphere in the 36-position sequence outlined above, and the high range-resolution of the SA16C mode, provide a number of new analysis opportunities to be examined. This mode was used in all DMSP experiments until 30 October 1995.

On and after 30 October 1995, the antenna mode was changed to the "World Day" mode, which is a nine-position/elevation scan mode. Figure 2 illustrates schematically an example of a DMSP/radar experiment carried out on 11 February 1996 using the World Day mode. Figure 2(a) is a display of the radar azimuth-elevation coverage by this radar mode and the DMSP footprint mapped along the magnetic field line to 125 km. Each pair of radar positions straddles the magnetic meridian as the elevation angle is changed to provide the extended coverage in magnetic latitude. After each cycle of nine positions, an elevation scan along the magnetic meridian is performed, and the cycle repeats. The elapsed time to complete 2.5 cycles

a. Azimuth – elevation coverage plot
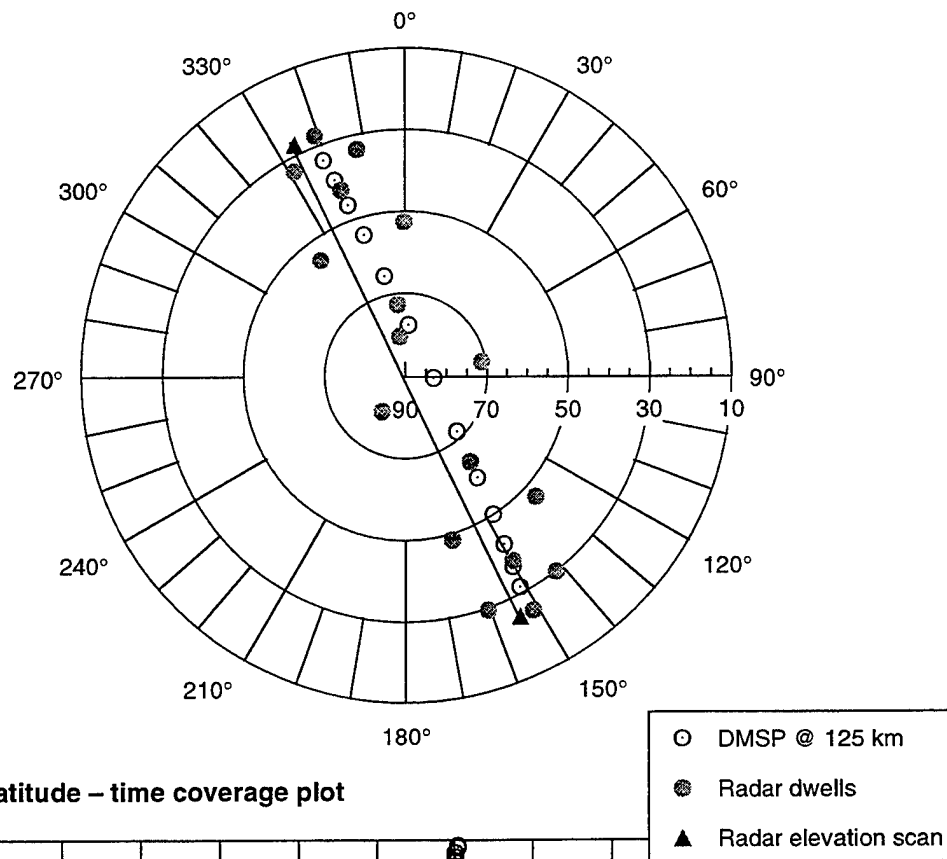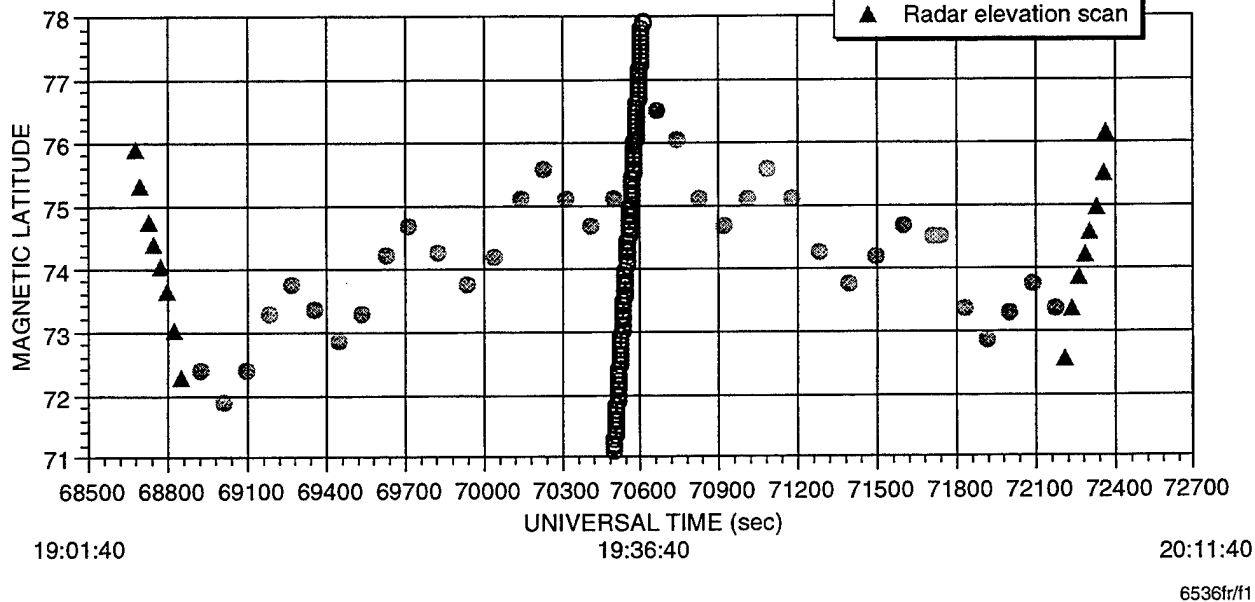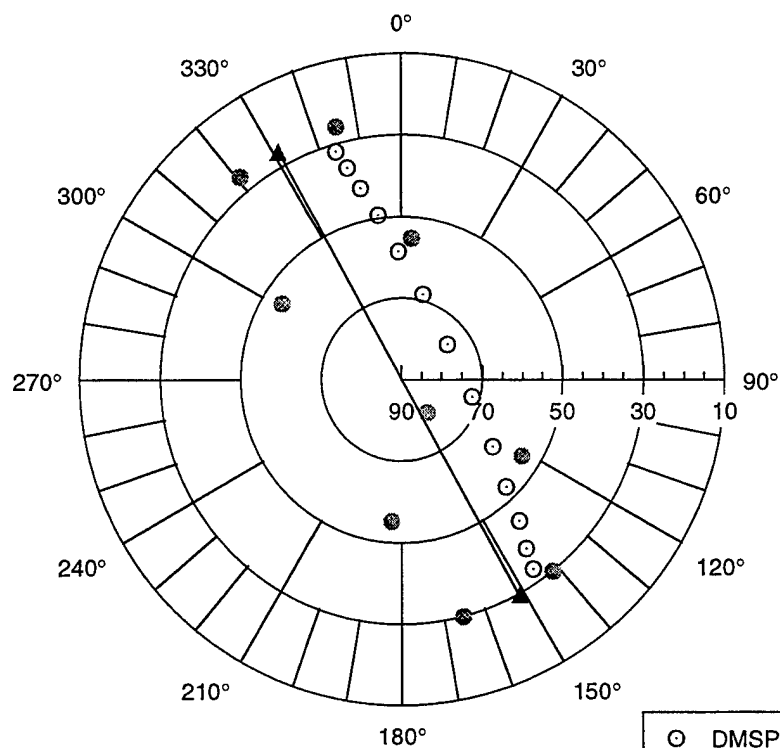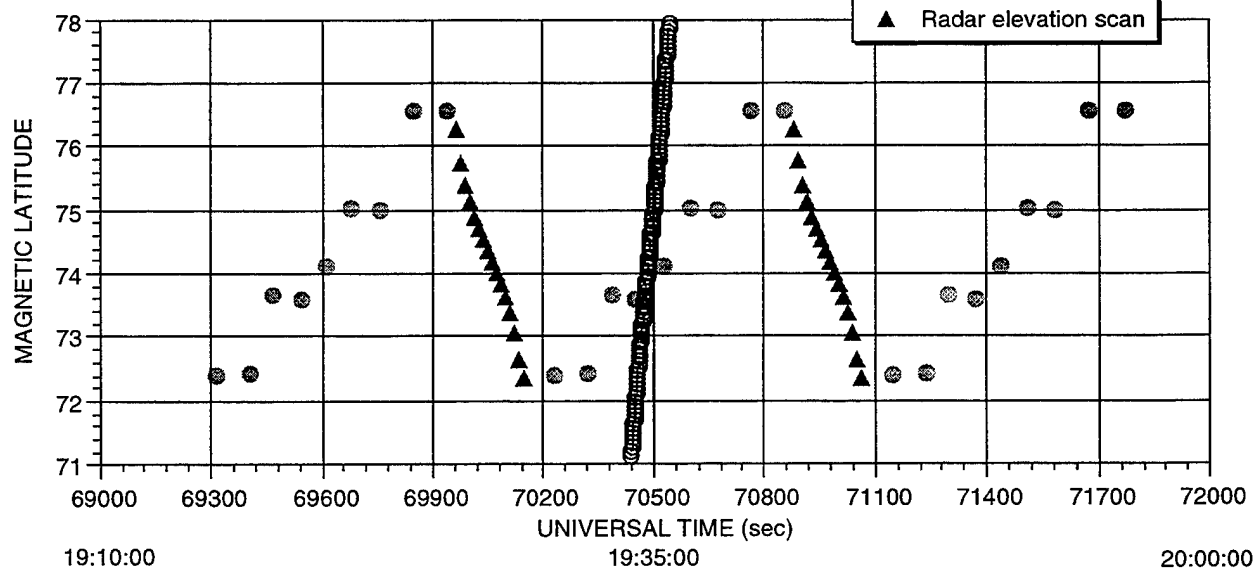

b. Magnetic latitude – time coverage plot

Figure 1   DMSP / RADAR EXPERIMENT: 2 AUGUST 1995

10

a. Azimuth – elevation coverage plot

b. Magnetic latitude – time coverage plot

Legend:
- ☉ DMSP @ 125 km
- ⬤ Radar dwells
- ▲ Radar elevation scan

6536fr/f2

Figure 2   DMSP / RADAR EXPERIMENT: 11 FEBRUARY 1996

11

of this mode and the magnetic latitude coverage is shown in Figure 2(b). Also displayed is the elapsed time of the DMSP pass for this day with respect to the radar measurement. Compared to Figure 1, this mode provides better temporal resolution than the DMSP mode but sacrifices in spatial resolution. Individual events using both of these modes are presented in Section 6 and the tradeoffs between modes are discussed.

5 METHODOLOGY

In the previous sections, we have described the overall approach of using the Sondrestrom incoherent-scatter radar to provide ionospheric measurements that will serve to validate the estimation of the Joule heating rate from measurements made by the F12 and F13 DMSP satellites. In this section, we will describe the methods used in the validation procedure.

5.1 Joule Heating Rate

The method used to derive the height-integrated Joule heating rate in the E-region ionosphere from DMSP measurements has been described by Rich et al. [1987, 1991]. The approach involves calculating the conductance and ionospheric currents along the same magnetic field line using DMSP satellite measurements of energetic particle precipitation by the SSJ/4 particle instrument and perturbation magnetic fields by the SSM magnetometer instrument. After some assumptions and use of empirical models, the height-integrated Joule heating rate is estimated from the expression

$$Q_j = \frac{J_P^2}{\Sigma_P} , \qquad (1)$$

where J_P is the height-integrated Pedersen current density and Σ_P is the height-integrated Pedersen conductance. The approach used to estimate the Pedersen conductance will be given in the next section. The Pedersen current is obtained from the simultaneously measured field-aligned current and the assumption that the majority of the field-aligned current is locally connected by the Pedersen current. This assumption is difficult to evaluate as it requires a two-dimensional mapping of the Hall and Pedersen conductance and electric field to determine the horizontal curl-free current. This approach has the added benefit of including the effects of the neutral wind in the estimation of the Joule heating rate. However, the manner in which (1) is evaluated assumes that the ionosphere is a flat slab with no height dependencies between the conductivity and the current.

Much work has been done using incoherent-scatter radars to quantify the dissipation rate of electromagnetic energy in the ionosphere through calculations of the Joule heating rate. Many of these investigations have used the expression

$$q_j = j_\perp \bullet E' = \sigma_p E'^2 = \sigma_p \left(E + u_n \times B \right)^2 , \qquad (2)$$

12

and have required the need to make some approximations to the Joule heating calculation. This is due to the fact that to evaluate accurately the Joule heating rate by (2), height integrated or not, requires knowledge of the electric field and the height distribution of the neutral wind and conductivity (requiring collision frequency and gyrofrequency calculations based on plasma and neutral composition). Quite often the neutral wind in (2) is assumed to be zero resulting in the approximate expressions for the local and height-integrated Joule heating rate given, respectively, as

$$q_j = \sigma_P E^2 \quad ; \quad Q_j = \int_{90}^{150} \sigma(z)_P E^2 \, dz = \Sigma_P E^2 \ . \tag{3}$$

This was the approach used in the previous radar/DMSP Joule heating study as described by Watermann and de la Beaujardiére [1990]. In that study it was generally assumed that the neutral wind was negligible and that a 48 km radar pulse was sufficient in describing the E-region electron density and, consequently, the conductance. As was shown in Scientific Report No. 1, the long pulse mode is not appropriate for estimating the E-region electron density and ion drift velocity when the E region is significantly structured, and can result in large systematic errors in estimating the Joule heating rate. We will also show in this report that the neutral wind is typically not negligible and can impact the actual Joule heating rate.

In Scientific Report No. 1 we described an alternate approach to estimating the local and height-integrated Joule heating rate from the radar measurements by using the expression

$$q_j = j_\perp \bullet E'_\perp = \frac{j_\perp^2}{\sigma_c} \quad ; \quad Q_j = \int_{90}^{150} \frac{j(z)_\perp^2}{\sigma(z)_c} dz \ , \tag{4}$$

where σ_c is the Cowling conductivity given by

$$\sigma_c = \sigma_P + \frac{\sigma_H^2}{\sigma_P} \ , \tag{5}$$

with σ_P and σ_H the symbols for the local Pedersen and Hall conductivity, respectively. Equation (4) is the more general expression of (1) but because this expression involves the difficult measurement of the local current density and the Cowling conductivity in the E region, many investigations have not used this approach. However, using (4) has the advantage that the effects of the neutral wind on the Joule heating rate are inherently contained within the current density measurement and the only significant model parameter needed in (4) is the collision frequency. The limitation to this approach is that it is applicable only for altitudes below about 150 km— although, below this altitude is where most of the heating is deposited. Given the new high-resolution mode this approach may used in the evaluation of the E-region Joule heating rate with much better accuracy than the previous DMSP study.

13

Test 1: An important comparison that may be done with the radar is to test assumptions that have been employed using (3) with the more accurate determination of the Joule heating rate using (4). In particular, the assumption of a zero neutral wind when using (3), as was done in the F7 DMSP/radar study, can be tested. To test this assumption, we do not require simultaneous DMSP measurements.

To address the impact neutral winds have on the Joule heating rate, we have analyzed radar data sets known to contain active periods with high electric fields. The local and height-integrated Joule heating rate were then estimated from these measurements using the expressions given by (3) and (4). Two days of extended radar measurements were used in the analysis. The first data set was taken on 5 August 1993 by the Sondrestrom radar using a three-position radar experiment (one position directed parallel to the magnetic field at 141° azimuth, 80° elevation, and the others 120° apart at 70° elevation) that employed the alternating code scheme discussed previously. Each position was integrated for 5 minutes and for two range gates, giving a range resolution of 6 km in the E region. The observations are representative of dayside auroral oval measurements covering the magnetic local time period from 05:49 to 19:49 with the solar zenith angle ranging from 82.8 to 77.5°, respectively and a maximum solar zenith angle of 50.1°. From these measurements, the resolved electric field and the E-region ion drift velocities resulting from the three position measurements and the mean E-region electron density were determined directly. We were then able to derive the current density and conductivity throughout the E region for this day using the high-resolution E-region data and the low-resolution F-region data for the electric field measurement. From these estimates, the height-integrated Joule heating rate, from 90 to 150 km, including neutral wind effects was calculated using (4). We then applied the derived Pedersen conductance from the high-resolution electron density measurements, height-integrated from 90 to 150 km, and the electric field measurement from the low resolution measurement to calculate the Joule heating rate, excluding neutral winds, using (3).

A comparison of these two forms for the local and height-integrated Joule heating rate calculations is shown in Figure 3 with panel (a) showing the height-integrated Joule heating rate using (3), solid orange line, and the height-integrated Joule heating rate using (4), solid black line. The height profiles used to determine the height-integrated Joule heating rates are provided in Figure 3(b). The profiles of the local Joule heating rate using (3) are presented in the bottom panel and profiles using (4) are presented in the top panel of Figure 3(b). The middle panel represents the difference between the bottom and top panels.

We will first discuss the height-integrated Joule heating rates presented in Figure 3(a). Here, we find two active periods during the experiment occurring near 10:00 and 18:00 UT. During the 10:00 UT period, we find relatively good agreement between the two approaches indicating that the neutral wind effect is small during this time. However, there is a significant departure between the two rates near 18:00 UT, which does indicate a neutral wind influence and an overall reduction of the actual Joule heating rate by almost 50%. The impact of the neutral wind to reduce the Joule heating rate is dependent on the time history of the neutral wind forcing.

14

a. Height-integrated Joule heating rates

b. Height-resolved Joule heating rates

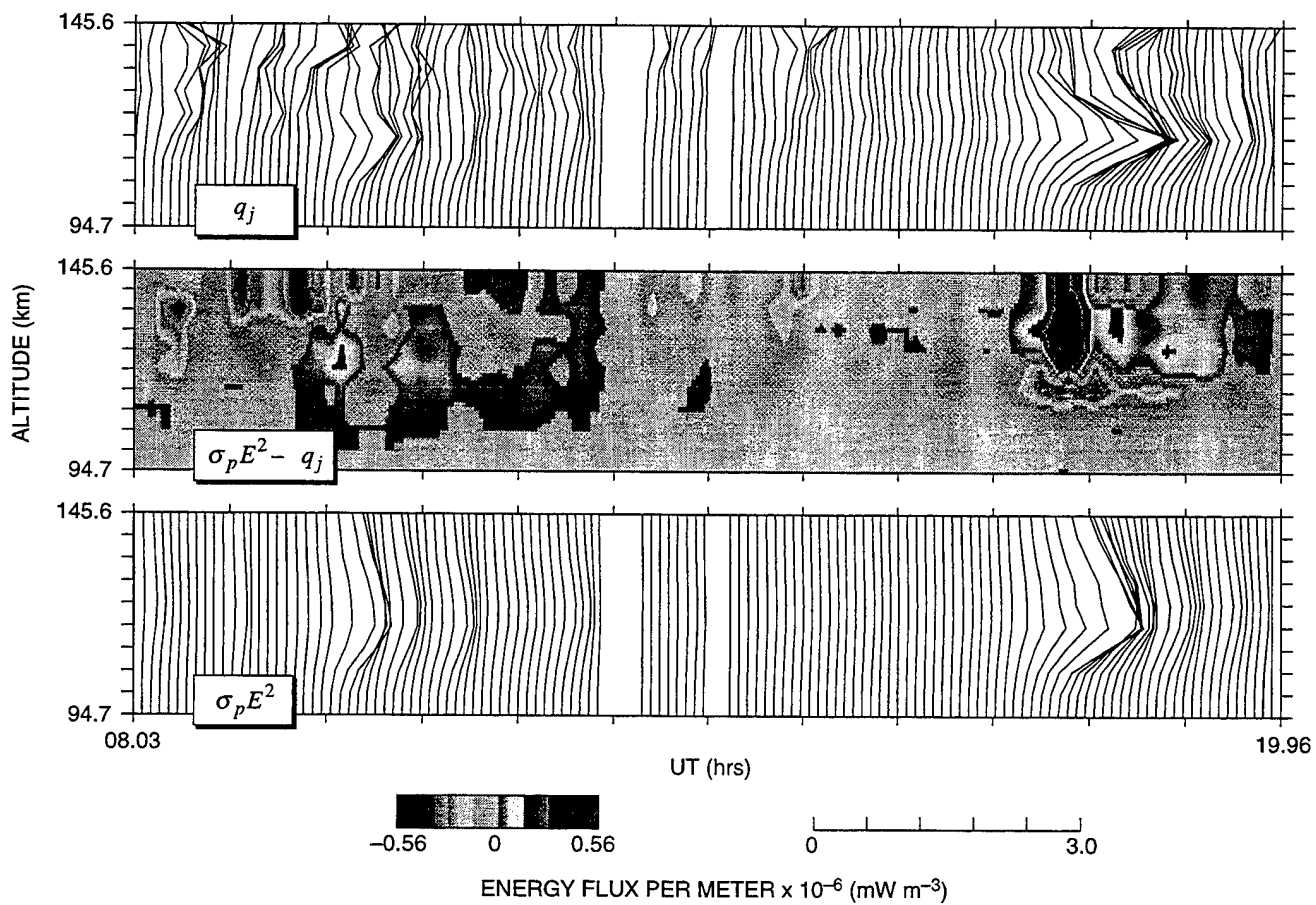ENERGY FLUX PER METER x 10^{-6} (mW m^{-3})
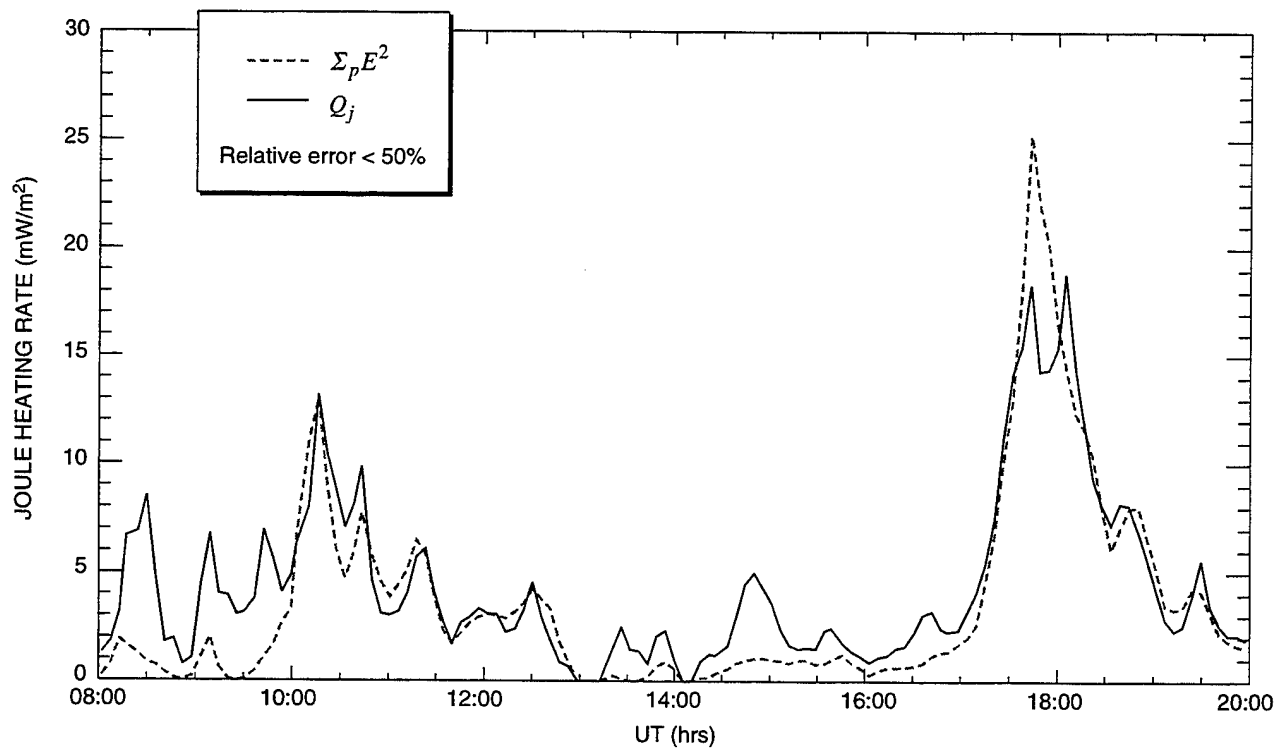
6536fr/f3

Figure 3   RADAR-DERIVED JOULE HEATING RATES: 5 AUGUST 1993

15

For the time period near 18:00 UT, the electric field magnitude increased but the direction of the electric field was constant since 15:00 UT. This would indicate that the neutral winds in the F region and topside E region have been forced by ion drag over a 3-hour period to flow in the direction of the ion drift and effectively reduce the Joule heating rate when the electric field magnitude increased.

Figure 3(b) shows the local effect of the neutral wind on the Joule heating rate. The shape of the profiles shown in the bottom panel reflect the vertical distribution of the Pedersen conductivity as the electric field is assumed to map without attenuation through the E region. This shape is modified in the top panel by the effects of neutral winds as the conductivity-weighted neutral wind contributes to the local Joule heating rate. Near 10:00 UT the middle panel, displaying the differences in profiles, shows both weakly positive and negative differences throughout the E region resulting in little influence of the neutral wind on the height-integrated Joule heating rate. Near 18:00 UT the middle panel shows a strongly positive difference in the upper E region becoming negative in the lower E region near 120 km. This would indicate that the wind is rotating in altitude as is typically the case at these altitudes. The positive difference on the topside indicates the neutral winds are moving opposite the electric field in a $-U_nXB$ direction, or, equivalently in the direction of the F-region ion drift. This neutral flow has the effect of significantly reducing the local Joule heating rate in the upper E region. As the altitude decreases the neutral winds begin to rotate in the direction of the electric field and the winds enhance the Joule heating rate in the lower E region. This enhancement can be seen in the middle panel by the negative difference depicted in blue and by the more localized Joule heating rate in the top panel peaking below 118 km with a width of only about 12 km. The reduction of the local Joule heating rate in the upper E region seems to indicate a penetration of strong convection-driven neutral wind flow in the F region into the upper E region. The constant direction of the electric field for the past 3 hours and the enhancement in the electric field magnitude at this time could be the reason for this penetration event.

The same analysis as above was performed on radar data taken on 2 May 1995. The mode was identical to the 5 August 1993 data set and the two forms of the Joule heating rate calculation for this day are presented in Figure 4. The panels in Figure 4 are of the same format as that presented in Figure 3. Figure 4(a) for this day shows weak Joule heating occurring between 7:00 and 9:00 UT followed by an extended period of enhanced Joule heating between 12:00 and 16:00 UT. During the period between 7:00 and 9:00 UT, the estimate of the height-integrated Joule heating rate from (4) often exceeds the estimate from (3) indicating that the neutral winds are acting to enhance the Joule heating rate. Within this time frame, the electric field magnitude peaked and then gradually reduced as shown by the solid orange line in Figure 4(a). What is not indicated in (a) is the variability in the direction of the electric field. From 6:00 to 11:00 UT the electric field changed direction by nearly 180° over nine times switching between a northward and southward electric field. This period indicates that the neutral flow cannot respond to such changes in electric field direction, which results in an

a. Height-integrated Joule heating rates

b. Height-resolved Joule heating rates

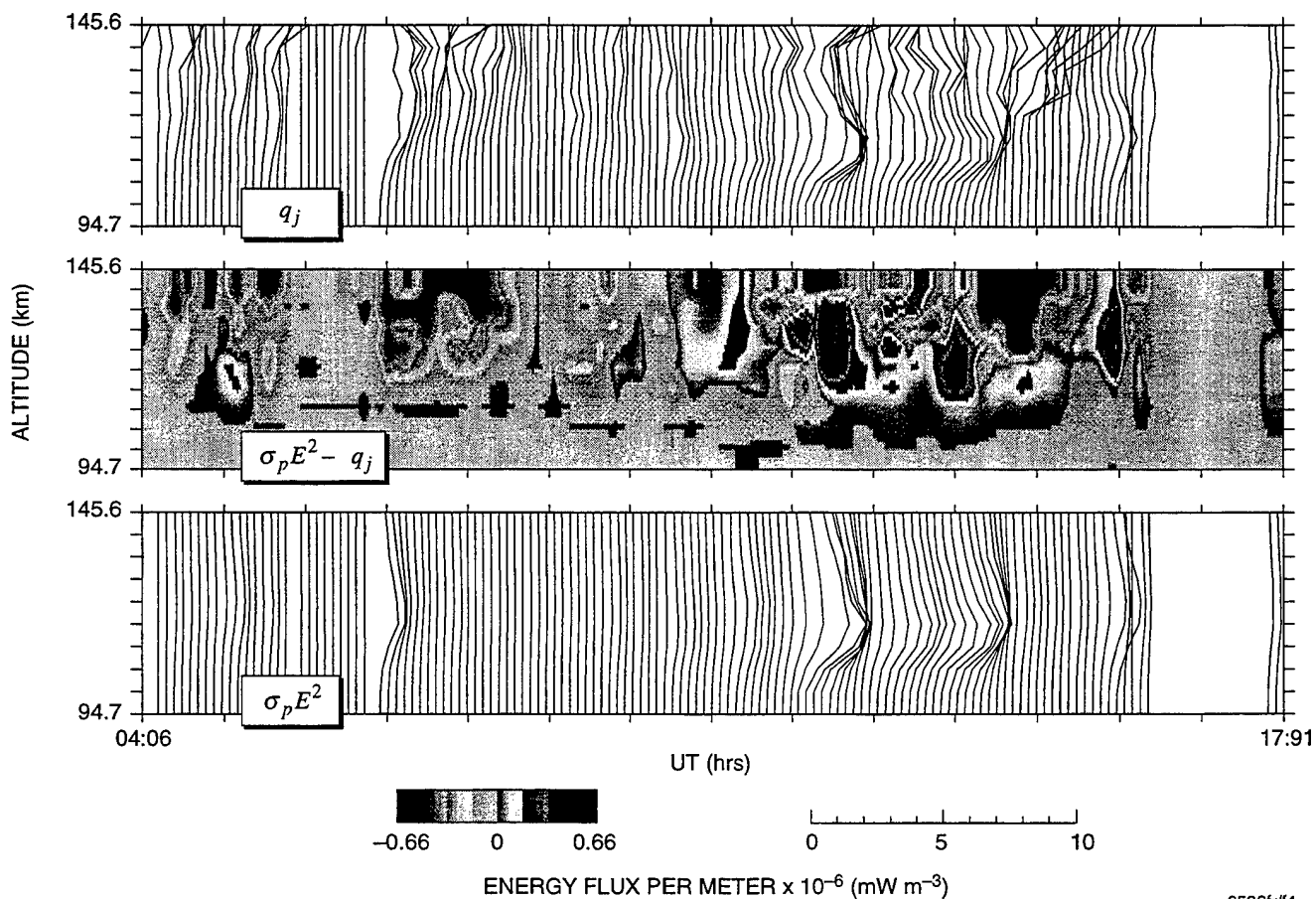ENERGY FLUX PER METER x 10^{-6} (mW m^{-3})

6536fr/f4
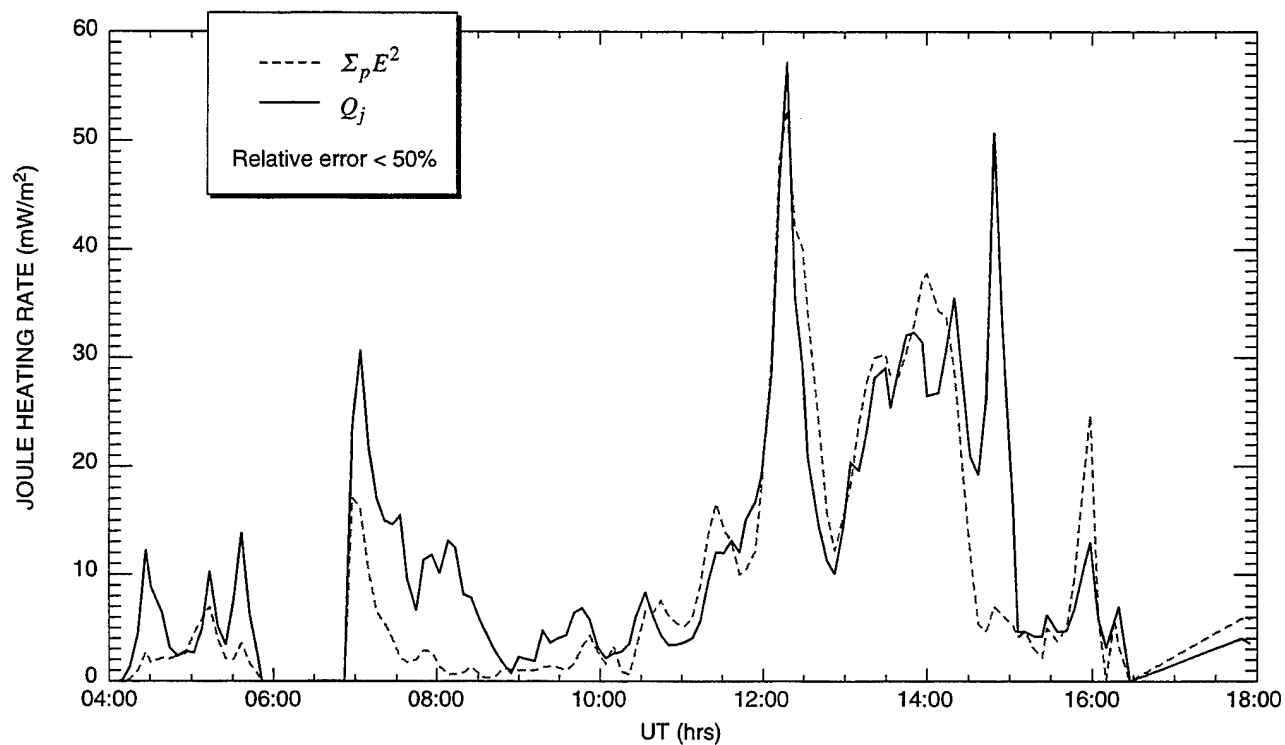
Figure 4   RADAR-DERIVED JOULE HEATING RATES: 2 MAY 1995

17

increase of the actual Joule heating rate. After 11:00 UT to about 14:30 UT the direction remained consistently southward and then after 14:30 UT switched to mainly a northward electric field until about 16:30 UT. As the direction of the electric field becomes more constant between 11:00 and 14:30 UT, the height-integrated Joule heating rate from (3) for the most part exceeds the calculation using (4), again establishing a reduction in the actual Joule heating rate due to neutral winds during times of constant electric field direction.

The Joule heating rate calculations following 14:30 UT are of particular interest as the electric field magnitude is significantly reduced and the direction of the electric field switches from southward to northward. During this period the calculation by (4) significantly exceeds the estimate using (3). Owing to the activity prior to this period it is expected that the neutral wind will be significantly enhanced requiring a number of hours to slow down. Due to this inertia and the change in electric field direction, the U_nXB direction of the neutral wind would complement the new electric field direction and enhance the Joule heating rate. The height-integrated Joule heating rates from (4) following 14:30 UT are an indication of this effect as the neutral winds are dominating the Joule heating rate.

Figure 4(b) shows the local effect of the neutral wind on the Joule heating rate for 2 May 1995. The middle panel illustrates that for the period between 7:00 and 9:00 UT the neutral wind contribution occurs in the upper E region. The period from 11:00 to 14:30 UT in the middle panel shows mostly negative difference values in the E region resulting in an overall reduction of the height-integrated Joule heating rate caused by the neutral winds. However, near 15:00 UT the difference values in the upper E region are strongly positive while at lower E region altitudes they become weakly negative. This pattern again shows a penetration event where the convection-driven neutral wind reaches the upper E region. In this case, the neutral wind is acting to enhance the Joule heating rate in the upper E region during a period when the electric field magnitude is reducing and the direction is changing. This case is opposite to that seen in the 5 August 1993 data set and is most likely due to the differing electric field behavior between the two days. That is, for the August 1993 data set the electric field magnitude is increasing with a steady direction while for the May 1995 data set the electric field was strong earlier and then reduced in magnitude and changed direction.

From these two data sets there seems to be an emerging picture as to the neutral wind impact on the Joule heating rate. Overall, the estimate of the height-integrated Joule heating rate using (3), that is, assuming the neutral wind is zero is, in general, a good proxy. However, there are times when the neutral wind can significantly impact the actual Joule heating rate. This impact seems to be associated with the time history of the electric field, as it is critical in forcing the neutral wind. Another important point is that the neutral wind contribution to the Joule heating rate is weighted by the local conductivity. That is, strong neutral winds can be present throughout the E region but its contribution to the Joule heating rate will be altitude dependent as the Pedersen conductivity decreases from the lower E region into the F region. Thus, the penetration events are strongly dependent on the conductivity as well as the neutral wind and

18

electric field. We also note that the typical rotation of the neutral wind with altitude in the E region can cause the impact on the Joule heating rate to be altitude dependent. This effect was seen in both of the cases presented. The most significant neutral wind contribution came after a substorm period on 2 May, 1995 resulting in an enhancement of the Joule heating rate by over 400%. Here the majority of the neutral wind contribution came from the upper E region, however, this was countered by a weak negative contribution in the lower E region. Neutral wind enhancements of the Joule heating rate by 200% were also observed during periods of significant changes in the electric field direction. Reduction of the Joule heating rate by neutral winds by as much as 50% were observed during periods of elevated magnitude in the electric field but with the direction of the electric field steady for extended periods.

Test 2: Because the new approach used to calculate the Joule heating rate by the radar is similar to that performed with the DMSP measurements, an assessment of the flat plate assumption can be made. To test this assumption, we again do not require simultaneous DMSP measurements.

At first inspection, it appears that there is very little difference between the DMSP approach given by (1) and the new radar approach given by (4) in estimating the Joule heating rate. It turns out, however, that there are subtle but important differences that need to be considered. First, the radar measures the total current density whose separation into Hall and Pedersen currents can only be done approximately because of the lack of information concerning the neutral wind direction. Second, integrating the local current density and Cowling conductivity independently with height is not a viable approach to estimating the height-integrated Joule heating rate. This is because the current density peaks in the E-region while the Cowling conductivity increases with height making the height-integrated quantity of (4) dependent on the local behavior between the Cowling conductivity and current density. This is further complicated by the fact that the neutral wind contribution is dependent locally on the con-ductivity as discussed above. The expression used in (1) has a related problem. If we first assume the neutral wind is zero, the Pedersen current and conductivity can be height-integrated independently to derive the Joule heating rate accurately using (1). This is because the shape of the Pedersen current profile with height, assuming zero neutral winds, is the same as the Pedersen conductivity profile. However, as soon as neutral winds are considered, the Pedersen current density height profile can differ from the Pedersen conductivity height profile and lead to an ambiguous result. We have already demonstrated in Figures 3 and 4 that the neutral wind can be significant with a varying influence with height. Thus, even though the DMSP approach used in (1) purports to include neutral wind effects through the measure of the height-integrated current density, the estimate of the height-integrated Joule heating rate is still somewhat uncertain because of the problem of taking the independent height-integration approach using (1).
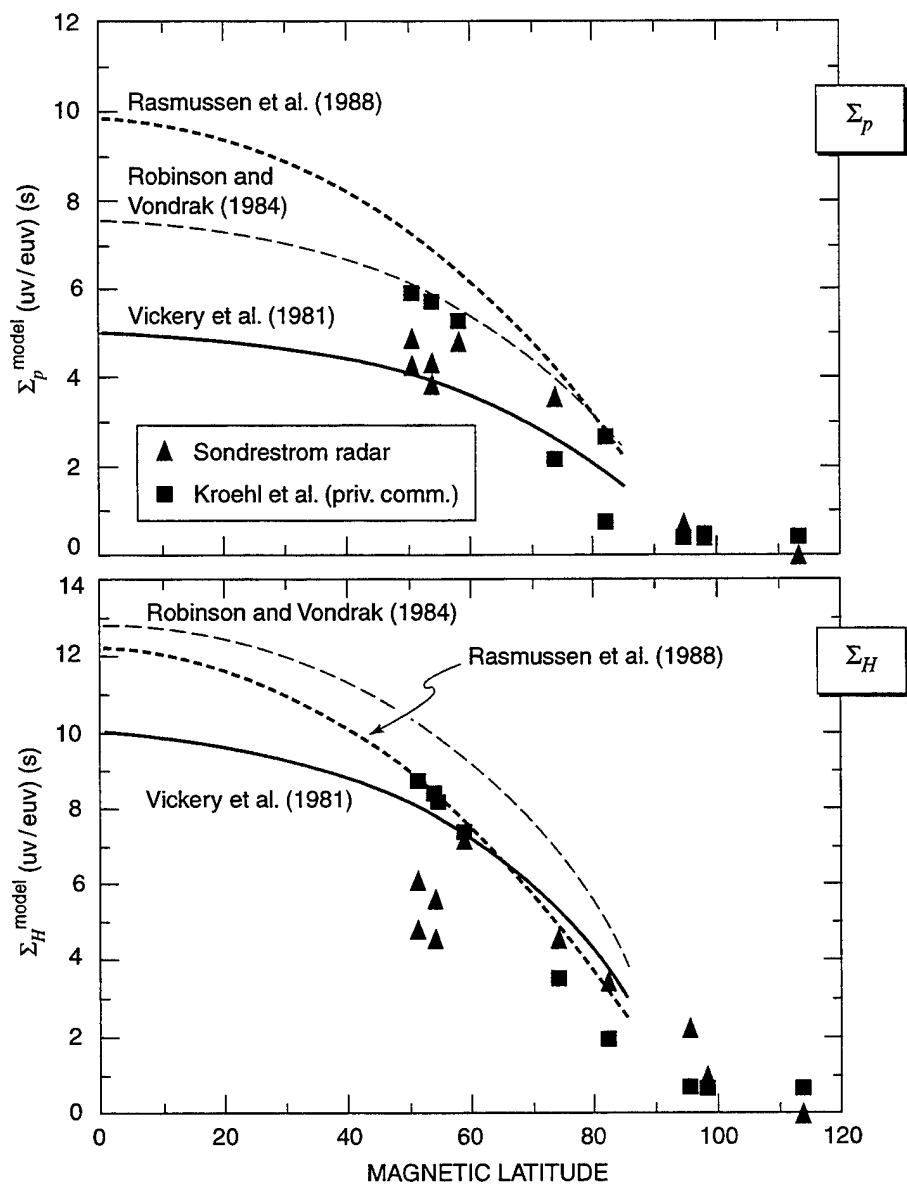
5.2 Conductance

The DMSP estimate of conductance assumes three sources of ionospheric ionization to be important: direct solar UV and EUV radiation, cosmic rays and galactic EUV, and the precipitation of energetic electrons downward along magnetic field lines. The solar-radiation produced term of the conductance is calculated from a formula given by Robinson and Vondrak [1984], with the 10.7-cm solar radio flux at 1 AU and the solar zenith angle as the governing parameters. A constant term of 0.1 mho is added to represent ionization from galactic sources.

The ionospheric conductance created by precipitating particles is estimated by assuming that the precipitating particles have certain characteristics [Robinson et al., 1987]. In particular, it assumes that the only flux is of downward electrons, the energy distribution is Maxwellian, and the particles are limited to an energy range between 500 eV and 30 keV. (This was true for the F7 study. For this study, the energy range was extended to 60 keV. Within these constraints, and under the assumption that the neutral atmosphere model is accurate, the conductivity and electron density can be estimated and can be compared to the radar-observed distributions. Robinson et al. [1987] have found that the particle distribution simplifications are appropriate, but the overall accuracy of the conductance depends on the proper choice of the energy limits between which the particle characteristics are computed and the proper velocity distribution of the precipitating particles.

Watermann et al. [1993] used the formulae of Robinson et al. [1987] to approximately separate the electron precipitation contribution from the radar-derived conductances in an attempt to isolate the photoionization contribution. They found the ionization of the atmosphere induced by solar UV and EUV is systematically overestimated by most available photoionization models, including the model by Robinson and Vondrak [1984] used in the DMSP calculations. The discrepancy between radar measurements and model calculations increases with decreasing solar zenith angle and, at least in the case of the Pedersen conductance, with increasing solar 10.7-cm flux and possibly with increasing geomagnetic activity. Figure 5 is a reproduction of Figure 3 from Watermann et al. [1993] that compares three photoionization models with radar data. We will use this figure to help evaluate the conductance estimates determined from our present study and to test the various photoionization models. The models presented in Figure 5 were evaluated for a 10.7-cm solar flux of 73, which matches the conditions for the current DMSP/radar data sets.

The formulae used to estimate the Pedersen and Hall conductivity from radar data in this study are the same as those described by de la Beaujardiére et al. [1991] and Watermann et al. [1993]. An important improvement has been in estimating the electron density in the E-region by the radar. As discussed in Scientific Report No. 1, pulse smearing effects by the long pulse waveform limit the accuracy in determining the electron density, particularly during strong energetic particle precipitation, and consequently impact the radar estimate of conductance. This systematic error is eliminated through the use of the short pulse waveform. To quantify the

20

Source: Waterman et al., 1993

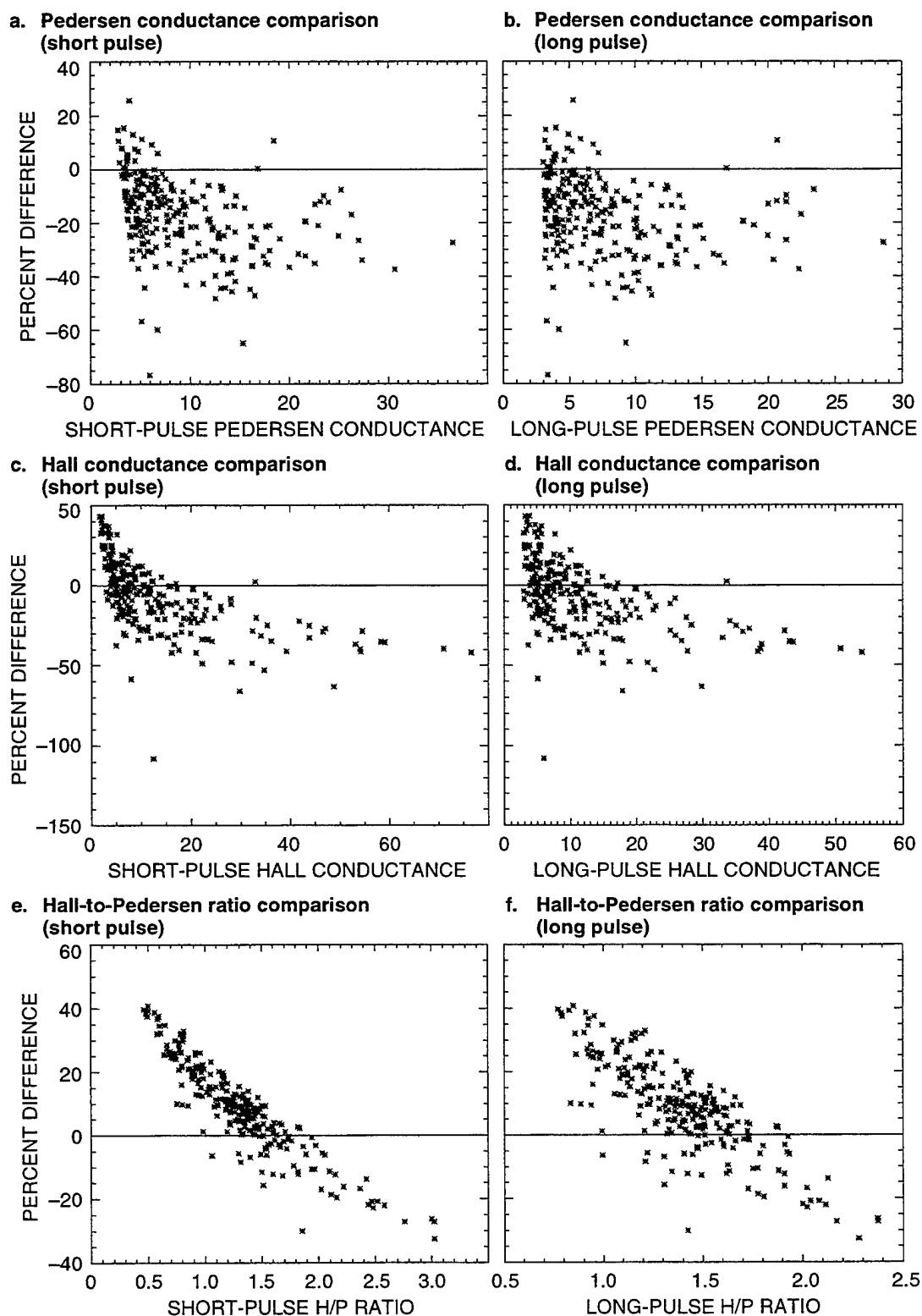**Figure 5 RADAR MEASUREMENTS OF Σ_p AND Σ_H**

impact of pulse smearing on the conductance estimates from long-pulse data, we have collected a number of radar data sets that used both the 3 km and 48 km pulse lengths. A total of 13 nights of experiments was included in the study and only positions fixed in the direction along the magnetic field line were used in the analysis. The data were filtered by solar zenith angle including only those measurements exceeding a solar zenith angle greater than 100°. After filtering, the Pedersen and Hall conductances are determined by height integrating the local conductivities from 90 to 300 km. In addition, the derived conductances are further filtered to include values greater than or equal to 3 mhos resulting in a total of 253 conductance values used in this study.

The long-pulse data provide an over sampled power measurement of the 48 km pulse every 2.1 km through the E and F region and autocorrelation functions (ACFs) containing information such as the electron density, plasma temperature and velocity every 21 km. Due to the coarse resolution provided by the long-pulse data of 21 km, the E region is poorly sampled and the resulting conductance estimate is often as bad as the pulse smearing effect. A common approach used to improve the E-region electron density resolution from the long-pulse data has been to approximately correct the power measurement made every 2.1 km. This is accomplished by fitting a spline to the temperature estimates made every 21 km and applying this continuous temperature function to the over sampled power measurement. This was the approach used by Watermann et al. [1993].

The short-pulse data provide independent power measurements and ACFs every 3 km through the E and F region. These measurements are void of pulse smearing and are used to compute the conductivity every 3 km when the fitting routine converges, otherwise, the short-pulse power measurement is used assuming the electron temperature and ion temperature are equal. From the short-pulse data we have computed the conductances and use these estimates to base the accuracy of the conductances computed using the spline-corrected power measurement of the long-pulse data.

Figure 6 illustrates the impact of pulse smearing by displaying the percent difference between the long-pulse and short-pulse estimates for the (a) Pedersen conductance, (b) Hall conductance, and (c) Hall-to-Pedersen ratio. On the left side of this figure (a, c, e), the percent difference is plotted against the short-pulse estimate of conductance with negative percent difference indicating an underestimate of the conductance values by the long pulse data. On the right side (b, d, f), the percent difference is plotted against the long pulse estimates, so that, these plots can be used to possibly correct the long pulse estimate.

For both the (a) Pedersen and (b) Hall conductances there exists quite a bit of scatter in the percent difference plots. This may be an indication that the conductances have a nonunique response to a range of precipitating particle events and/or pulse smearing of the plasma temperature used in corrected the electron density is variable. For the Pedersen conductances beyond 5 mhos the long pulse underestimates the actual value by as much as 40%. The Hall

a. Pedersen conductance comparison (short pulse)

b. Pedersen conductance comparison (long pulse)

c. Hall conductance comparison (short pulse)

d. Hall conductance comparison (long pulse)

e. Hall-to-Pedersen ratio comparison (short pulse)

f. Hall-to-Pedersen ratio comparison (long pulse)

6536fr/f6

Figure 6   EVALUATION OF PULSE SMEARING EFFECTS ON CONDUCTANCE ESTIMATES

23

conductance overestimates the actual conductance below about 5 mhos and systematically underestimates the actual conductance beyond 15 mhos. The trend in the Hall conductance seems to show that the long pulse estimate worsens as the actual Hall conductance increases and at large values could underestimate the Hall conductance by as much as 40 to 50%. The Hall-to-Pedersen ratios displayed in (e) show a near linear relation between the percent difference and the short pulse Hall-to-Pedersen ratio. The trend in the Hall-to-Pedersen ratio shows the long pulse to overestimate the ratio for values less than 1.5 while underestimating the ratio for values exceeding 1.5. The trend also indicates that for energetic events with the ratio exceeding 3.0 the long pulse would underestimate the ratio by 40% or more.

Quite often the short-pulse data are not available to permit better estimates of the conductivity. In these circumstances, the long-pulse data must be used and the impact of using such data on conductance estimates has been shown above to be important. Thus, it is worthwhile to show the relationship of the percent difference of the long pulse to short pulse estimates of conductance versus the long pulse estimate as presented on the right hand side of Figure 6 (b, d, f). That way, an independent long pulse measurement can be made and possibly corrected based on this plot. Here we find more scatter in percent difference in all the plots but with similar trends as were observed in Figure 6 (a, c , e). Crude corrections can be made to individual Hall and Pedersen conductances estimates from long-pulse data using plots (b) and (d). A much better relationship seems to still exist concerning the Hall-to-Pedersen ratio and corrections using (f) can be made from long pulse estimates of the ratio to improve its accuracy.

In summary, the pulse smearing effect produced by applying long-pulse waveforms in the E region results in a systematic error in estimating the actual conductance. Trends shown in Figure 6 allow crude corrections to be made to the long pulse estimates. For estimating the Joule heating rate from long pulse data, the Pedersen conductance can be underestimated by 20 to 30% which would lead to an equivalent underestimate in the Joule heating rate calculation. Because Watermann and de la Beaujardiére [1990] used this approach, their results are most likely an underestimate of the actual Joule heating rate.

The data presented in Figure 6 represent conductances created solely by particle precipitation. This type of ionization will cause a larger variability in the pulse smearing effect due to the variable structuring of the E region. For daytime observations pulse smearing seems to be less of a factor mostly due to the rather uniform distribution of the E-region electron density with height.

6 ANALYSIS OF INDIVIDUAL DMSP/RADAR EVENTS

We have selected six of the 39 DMSP/radar experiments for further radar analysis and comparison with DMSP measurements. Radar-derived Pedersen and Hall conductances and the Joule heating rates for these six experiments have been determined. This section will detail the DMSP/radar measurements for these six experiments and provide comparisons between the DMSP estimated conductance and that derived by the radar. The Joule heating rates from the radar measurements will also be included, when of satisfactory magnitude, in anticipation of future comparisons with the Joule heating rate estimates from the DMSP measurements when they become available. Table 3, along with Tables 1 and 2 presented earlier, lists the specific details and conditions for the six selected DMSP/radar experiments. The columns in Table 3 represent (from left to right) the year with day number, the date in yymmdd format, the start time of the radar experiment, the end time of the radar experiment, the DMSP satellite, the highest elevation angle seen by the radar of the DMSP satellite after projecting the footprint along the magnetic field line to an altitude of 125 km, the UT time of the DMSP at its highest elevation angle, and the solar zenith angle for that time and at an altitude of 125 km. The first three experiments represent summertime, sunlit conditions while the last three occur in the wintertime under twilight conditions. All experiments were taken during solar minimum conditions with an average $F_{10.7}$ of less than 80.

Table 3. Select DMSP Passes for Comparison with Radar Observations

Day No.	Date	Radar Start UT	Radar Stop UT	Satellite	Elev Angle	DMSP Pass Time UT	SZA
(95) 155	950604	1910	2012	f13	82.6	19:38:10	59.36
(95) 197	950716	1854	2008	f13	83.5	19:38:15	59.68
(95) 214	950802	1850	2006	f13	83.0	19:35:50	62.90
(96) 008	960108	1751	2103	f13	75.7	19:40:40	100.45
(96) 042	960211	1726	2100	f13	75.8	19:34:50	91.37
(96) 050	960219	1801	2102	f13	81.4	19:39:20	89.57

In the following subsections we present detailed comparisons for the six events. To provide a proper comparison between the inherently coarser resolution of the radar position measurements with the high-resolution measurements by DMSP, we have performed a running mean on the DMSP data covering 0.5° of magnetic latitude prior to making the comparison. This was performed on five of the six experiments. It should be noted that for all experiments only the particle precipitation contribution has been included in the DMSP estimates of conductance. This will allow us to evaluate the solar photoionization contribution to the radar measurements and test the results of Watermann et al. [1993]. Also, only 1 day of Joule heating estimates was

25

included because the other days either had low electric fields or E-region estimates of the electron density and ion drift were poor.
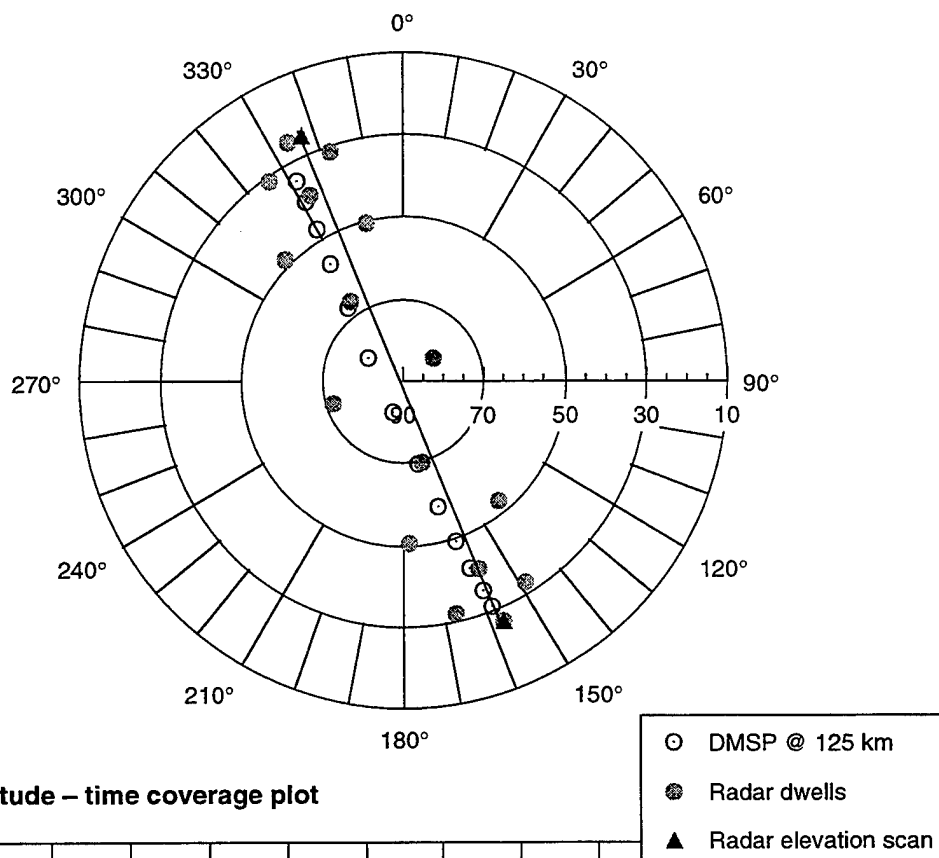
6.1 4 June 1995—Day Number 155

For this experiment the geomagnetic conditions were rather quiet but sufficient E-region electron density due to solar photoionization was present to provide good signal statistics. This day was chosen to test the conclusions presented by Watermann et al. [1993] that were discussed in Section 5. The DMSP/radar azimuth-elevation coverage and the magnetic latitude-time coverage for this day are presented together in Figure 7. The DMSP radar mode, described in Section 4, was used for this day. A general description for this type of figure was given previously in Section 4. The satellite pass was very close to the magnetic meridian and excellent spatial overlap with the radar was obtained, as designed by the radar mode. The closest time when DMSP and radar measurements were being made occurred near 75.5° magnetic latitude.

The Pedersen and Hall conductances from the radar position measurements taken during the first and second half of the experiment are compared with the smoothed DMSP conductance estimates in Figure 8(a) and (b), respectively. An inset in Figure 8(a) shows the actual resolution provided by the DMSP measurement. The abrupt drops in the radar-derived conductance near 72° and 77° are artificial and result from limited radar coverage of the E region. The magnetic latitude range between 72.5 and 76° are optimal as they correspond to an altitude of 100 km for the lowest radar elevation angle near 30°. Very little change in the radar estimates of conductance is seen over the entire hour of observation and is representative of conductances produced by solar photoionization. The DMSP conductance estimates are only for particle precipitation and show that for this pass the contribution of precipitating particles to the conductance is low.

As very little change is seen in the radar measurement, it appears that the conductance is dominated by solar photoionization and lends itself for comparison with solar photoionization models, as was done in Watermann et al. [1993]. The idea presented by Watermann et al. [1993] was to evaluate the ability of these models to reproduce the observed radar conductances during known times (provided by the DMSP measurements) of weak or no particle precipitation. We will use the same approach but, due to the significant temporal differences between the two measurements, we will also base our results on the behavior of the radar conductance estimates taken over the hour.

At the start of the experiment, the solar zenith angle was 57.0° and at the end of the experiment an hour later it reached 62.1°. From Figure 8 we find radar conductances typically near 6 mhos for Pedersen and 6.5 mhos for Hall. Using Figure 5 and a solar zenith angle of 60°, we find the Robinson and Vondrak [1984] model for the Pedersen conductance to be very close to about 5.5 mhos and matches nicely with the radar estimates given in Figure 8. The Hall

a. Azimuth – elevation coverage plot
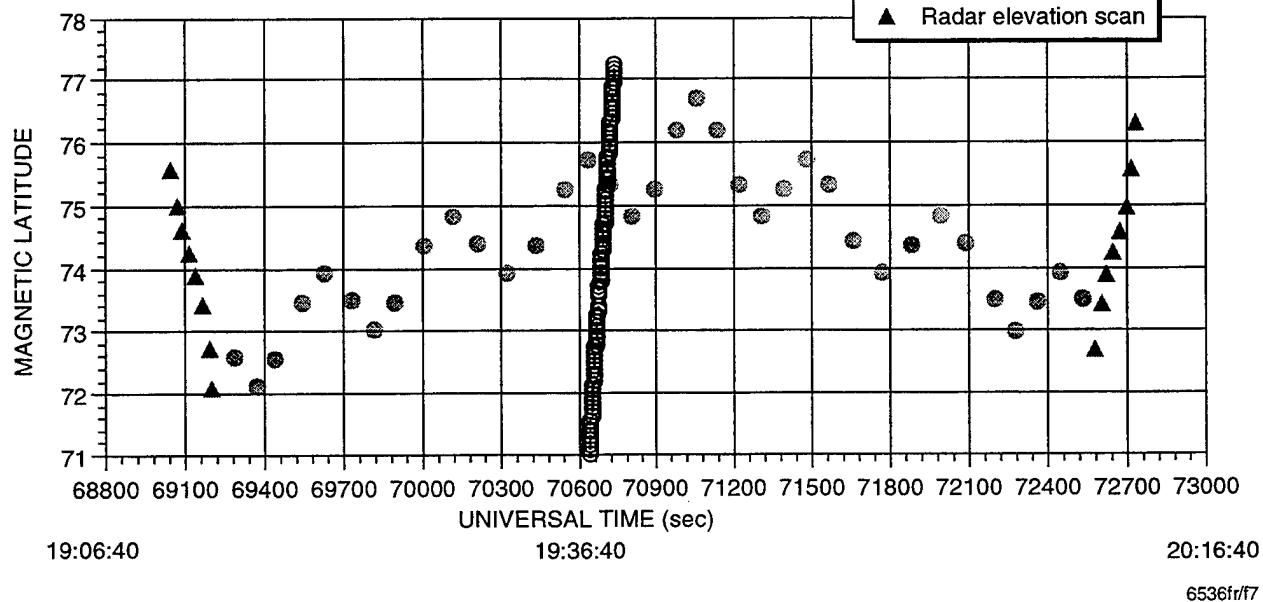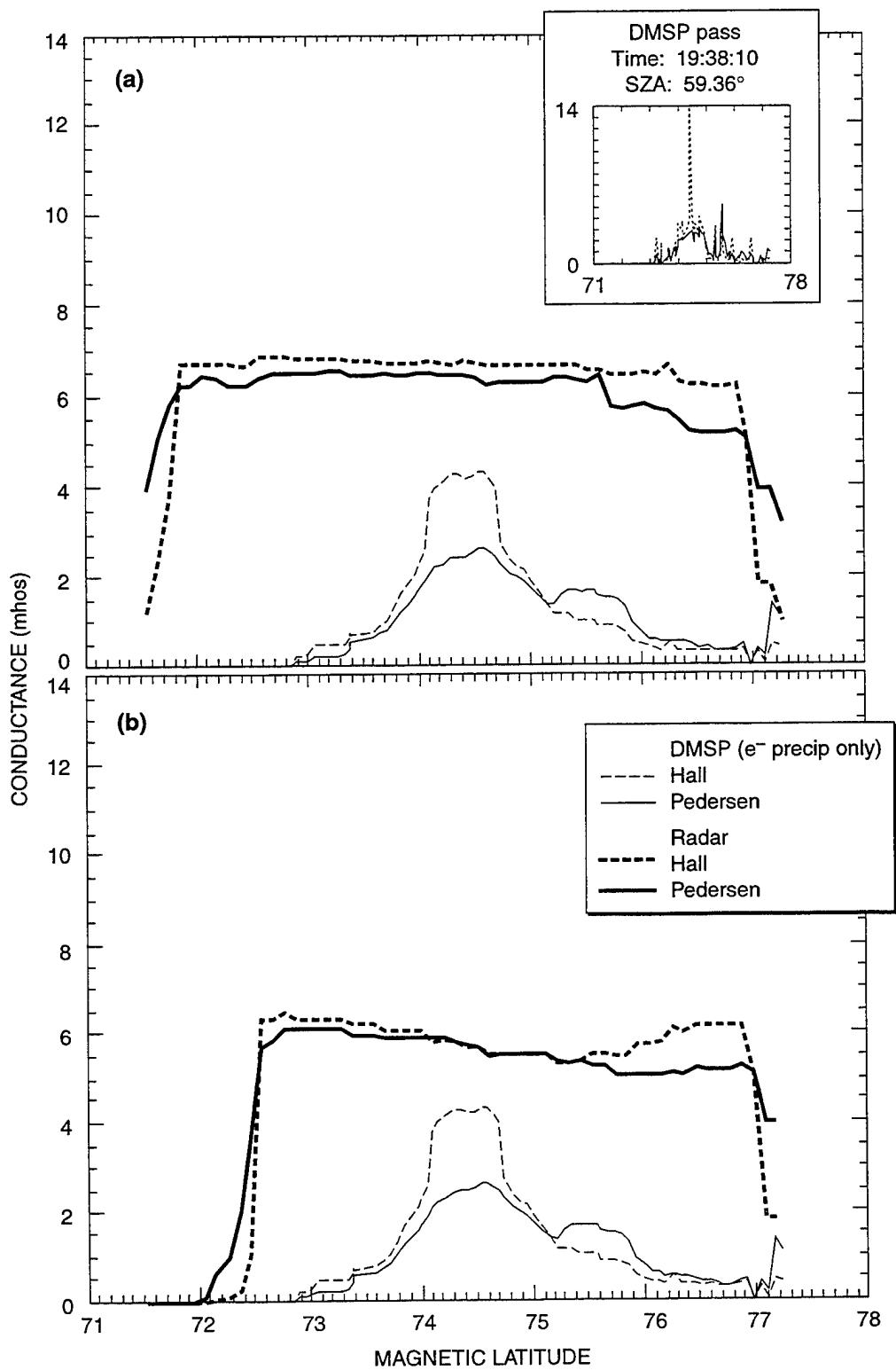

b. Magnetic latitude – time coverage plot

Legend:
- ⊙ DMSP @ 125 km
- ◉ Radar dwells
- ▲ Radar elevation scan

19:06:40   19:36:40   20:16:40

6536fr/f7

Figure 7   DMSP / RADAR EXPERIMENT: 4 JUNE 1995

27

Figure 8   DMSP/RADAR CONDUCTANCE COMPARISONS: 4 JUNE 1995

6536fr/f8

28

conductance modeled by Robinson and Vondrak [1984] is near 9 mhos and, thus, overestimates the radar estimate by 30%. The Hall conductances modeled by Vickrey et al. [1981] appear to be more in line with the radar estimates of the Hall conductance for this day.

These results are in better agreement with the photoionization models than the Watermann et al. [1993] study. We reproduced their approach in estimating the conductances and applied it to the same data set as above to determine if the difference could be explained by pulse smearing caused by the long-pulse waveform used in their study. We found the conductance estimates using the Watermann et al. [1993] approach for this day underestimated our estimate of conductance by 10 to 15%. This would bring their results more in line with our observations for this day.

6.2 16 July 1995—Day Number 197

The DMSP/radar azimuth-elevation coverage and the magnetic latitude-time coverage for this day are presented together in Figure 9. Again, the spatial overlap of the radar and satellite footprint is very good. The closest coincidence between the two measurements occurs near 76° magnetic latitude on the first half of the radar experiment as shown by Figure 9(b).

The Pedersen and Hall conductances from the radar position measurements taken during the first and second half of the experiment are compared with the DMSP conductance estimates in Figure 10(a) and (b), respectively. As the radar measurement progresses in Figure 10(a) from 72 to 77° there is an increase in the overall conductances from what is believed to be produced by precipitating particles in addition to photoionization. This particle precipitation increase is confirmed by the DMSP measurements that show an increase in conductance with increasing latitude. The radar conductances from the other half of the radar experiment shown in Figure 10(b) continue to show elevated conductances through all latitudes of coverage and would indicate a spatially broad or temporally varying particle precipitation source. Due to the scale of the DMSP conductance estimates and the long time to complete a north-south cycle in this radar mode, it seems a temporal variability would be the most probable cause of the enhanced conductance at all latitudes in Figure 10(b).

The solar zenith angle for this day of 60° is very close to that for 4 June 1995, and so the same Robinson and Vondrak [1984] model values of 5.5 mhos for Pedersen conductance and near 9 mhos for the Hall conductance are applied. If we consider the radar estimate of conductance in Figure 6(a) to be solar produced near and equatorward of 74°, the modeled solar contribution to the Pedersen conductance is in good agreement with the radar measurement. The modeled solar contribution for the Hall conductance is overestimated from the observations again by about 30%. Keep in mind that although the addition of the solar contribution to the DMSP estimate would bring values equatorward of 74.5° into better agreement, the precipitation feature between 74.5 and 76° would be enhanced over the estimate provided by the radar.

a. Azimuth – elevation coverage plot
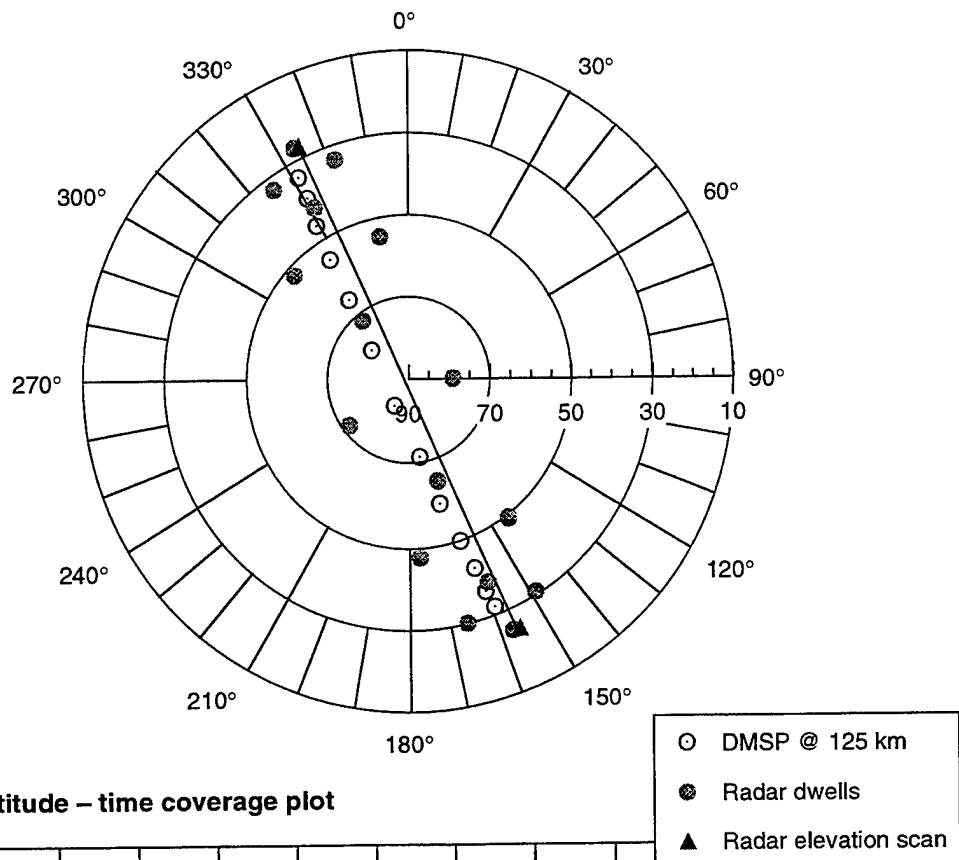
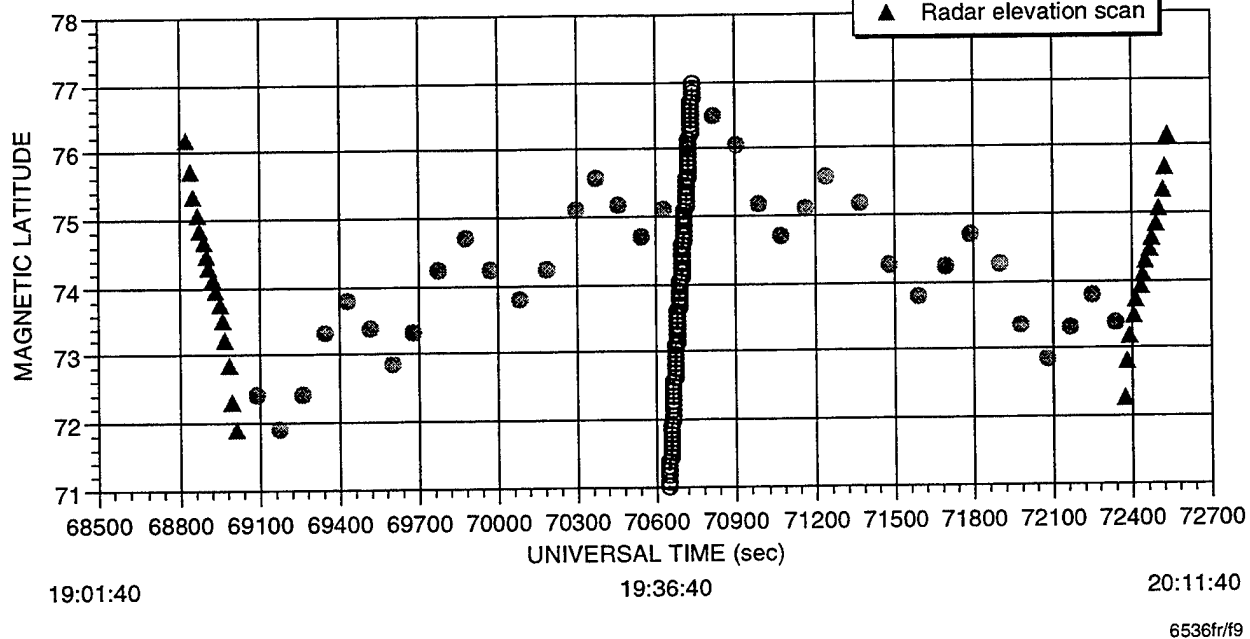## b. Magnetic latitude – time coverage plot

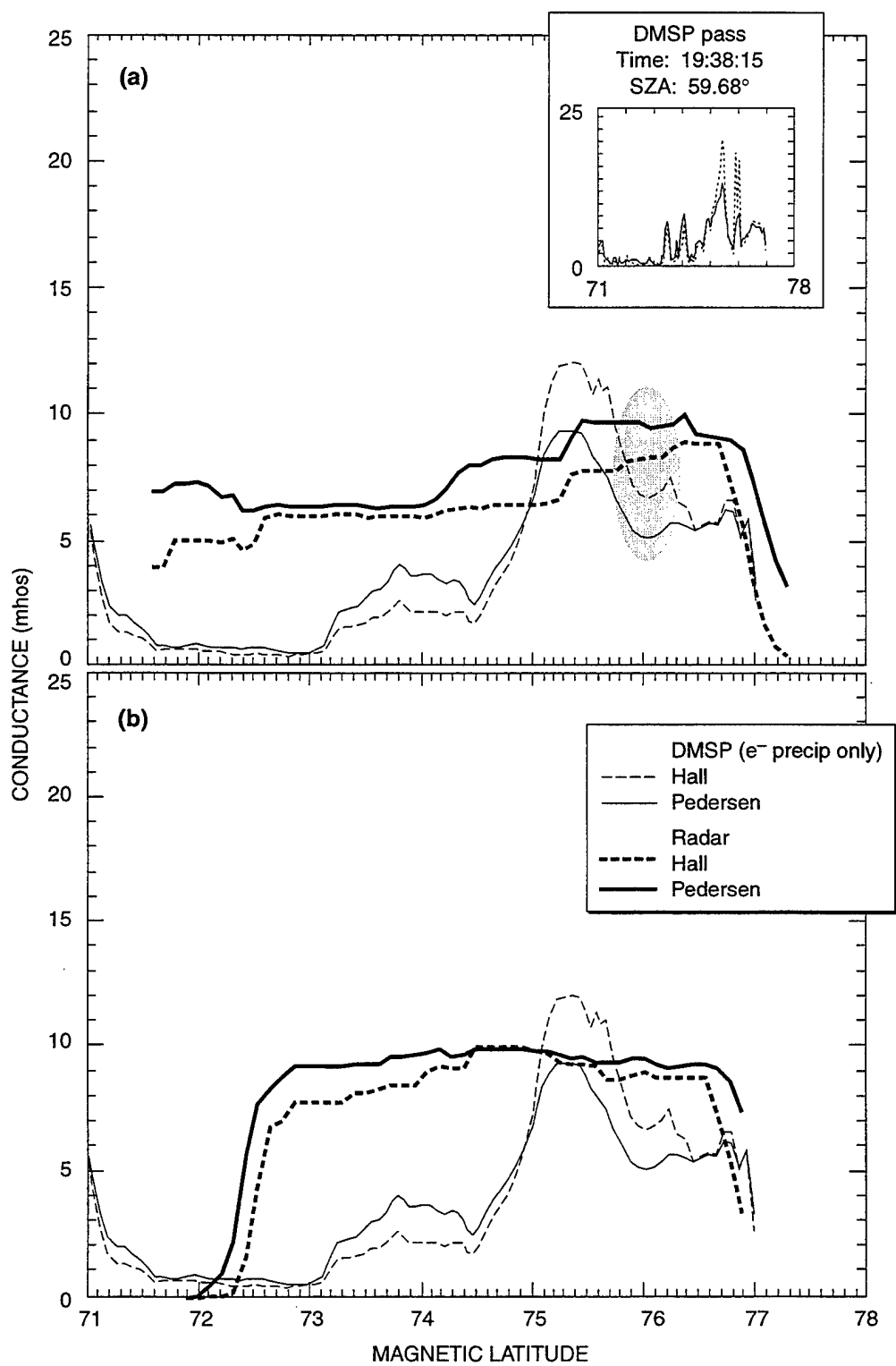**Figure 9 DMSP / RADAR EXPERIMENT: 16 JULY 1995**

30

Figure 10   DMSP / RADAR CONDUCTANCE COMPARISONS: 16 JULY 1995

31

The data taken near closest coincidence are circled in Figure 10(a) near 76° to examine the conductance estimates at the best spatial and temporal coincidences of the two measurements. At this location the DMSP data show a reduced level of particle precipitation contributing to the conductance. Adding the contribution due to solar photoionization, the Pedersen conductance from DMSP compares well with the radar while the Hall would be significantly overestimated.

The radar estimate for the height-integrated Joule heating rate is presented in Figure 11. This is the most active case of all of the six experiments and the only one worthy to show. The Joule heating rate peaks near 74° exceeding 80 mW/m^2. This would be a good case for comparison with DMSP.

6.3 2 August 1995—Day Number 214

The DMSP/radar azimuth-elevation coverage and the magnetic latitude-time coverage for this day were presented previously in Figure 1. Again, the spatial overlap of the radar and satellite footprint is very good, by design. The closest coincidence between the two measurements occurs near 76° magnetic latitude on the first half of the radar experiment as shown by Figure 1(b).

The Pedersen and Hall conductances from the radar position measurements taken during the first and second half of the experiment are compared with the DMSP conductance estimates in Figure 12(a) and (b), respectively. The DMSP conductances show enhancements near 72°. The radar estimates in Figure 12(a) show only a weak indication of particle precipitation near 73° with the majority due to solar photoionization. Figure 12(b) also shows conductances largely created by photoionization. Over the time it takes this particular radar mode to cover magnetic latitudes from 72 to 76° and back to 72° the solar zenith angle changed from 57.1 to 62.5°. If we evaluate the solar photoionization contribution during low activity for solar zenith angles near 60°, we find that the Pedersen conductance due to solar photoionization of 5.5 mhos is in good agreement with the Robinson and Vondrak [1984] model. The Hall conductance is again overestimated by Robinson and Vondrak by about 30% as was found on the 4 June and 16 July data set. The Vickrey et al. [1981] model does a better job in reproducing the solar photo-ionization contribution to the Hall conductances for the three days presented here.

6.4 8 January 1996—Day Number 008

The DMSP/radar azimuth-elevation coverage and the magnetic latitude-time coverage for this day are presented together in Figure 13. Here, the World Day antenna mode was used in the experiments to improve the temporal versus spatial resolution of the measurement. Because the World Day mode is designed to align the positions along the magnetic meridian, the satellite footprint and the radar positions do not overlap spatially. On the magnetic latitude-time plot, the time scale is much shorter than the previous mode and so the temporal resolution of the magnetic latitude coverage is improved. The closest coincidence between the two measurements occurs
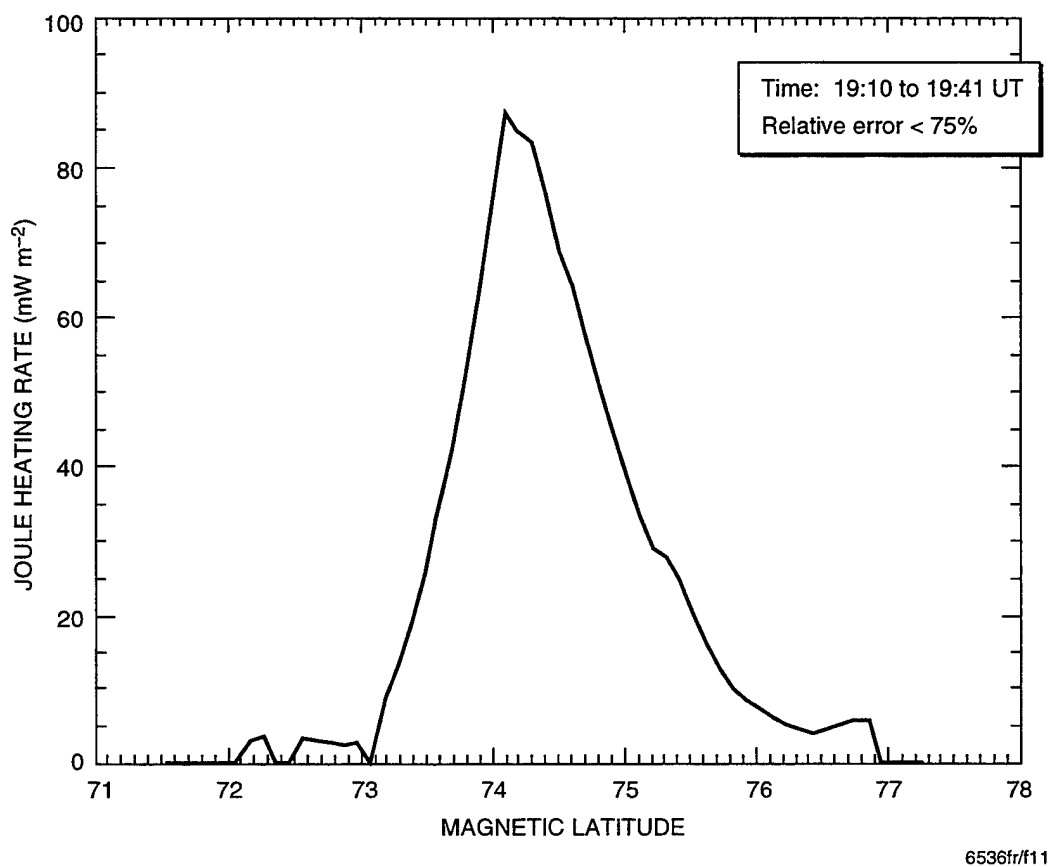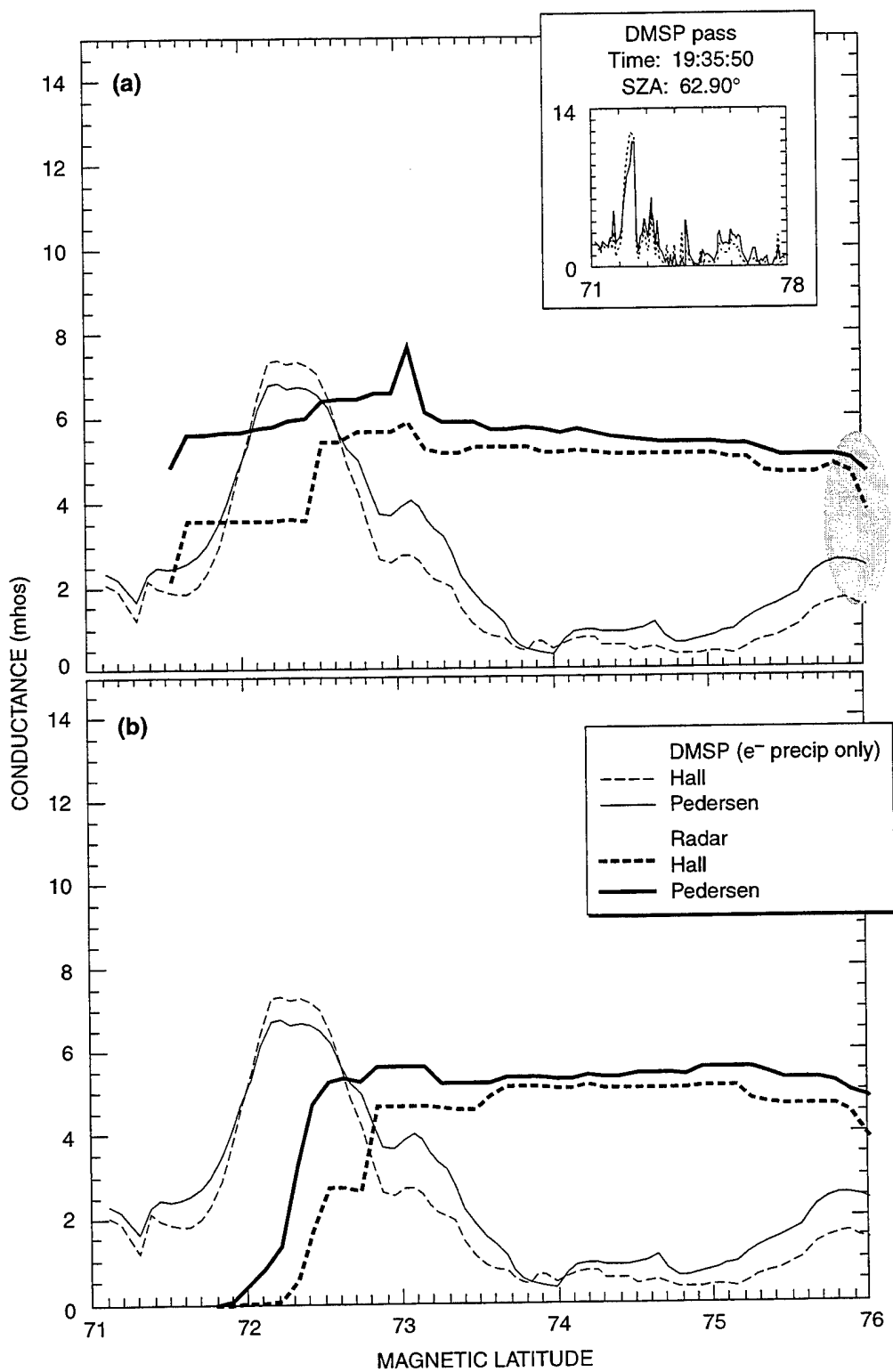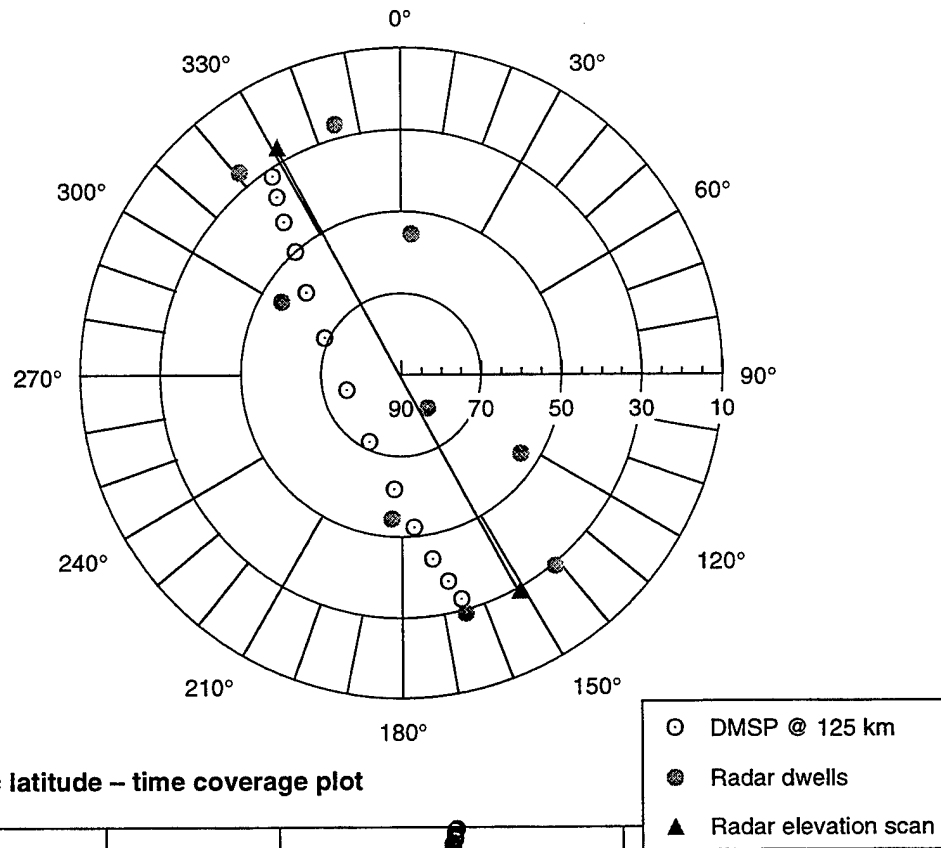
Figure 11   RADAR JOULE HEATING RATE ESTIMATE: 16 JULY 1995

Figure 12 DMSP / RADAR CONDUCTANCE COMPARISONS: 2 AUGUST 1995

6536fr/f12

a. Azimuth – elevation coverage plot

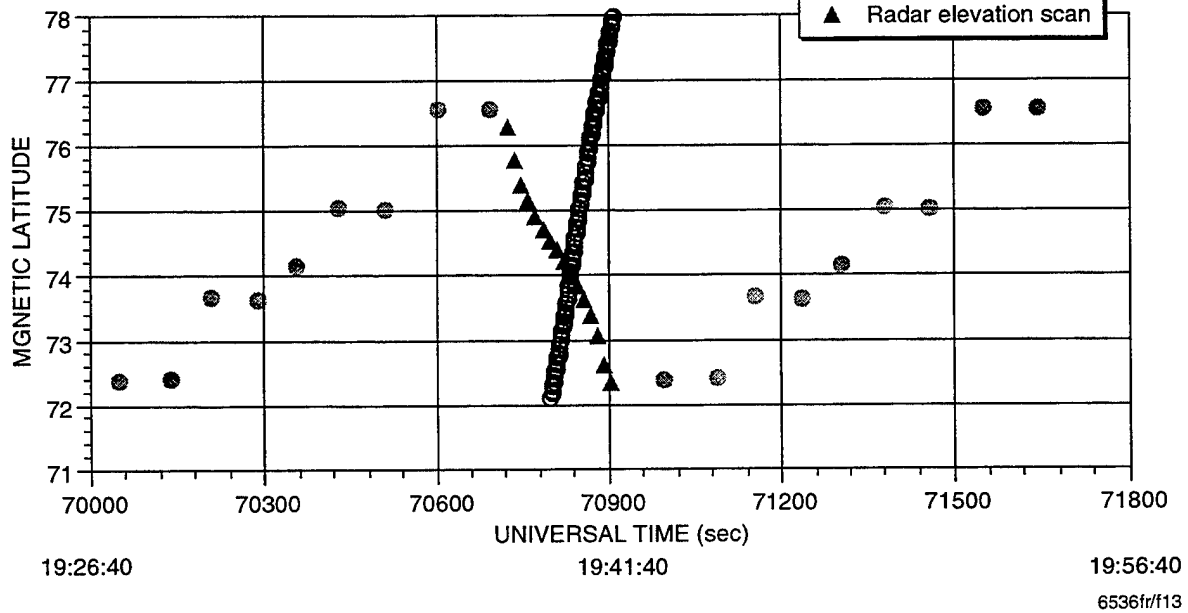## b. Magnetic latitude – time coverage plot

Figure 13   DMSP / RADAR EXPERIMENT: 8 JANUARY 1996

35

during an elevation scan near 74° magnetic latitude with at most a 2-minute difference at other latitudes. The solar zenith angle for this day is near 100° at 125 km altitude and represents our only data set where particle precipitation is the primary contributor to E-region ionization.

Figure 14(a) compares directly the radar estimates of conductance from the elevation scan with the DMSP conductance estimates. No smoothing has been applied to the DMSP data because the radar elevation scan provides good spatial resolution for direct comparison. The sharp decrease in the radar estimate of conductance near 73° is artificial and due to the limited E-region coverage of the scan. It should be noted that the conductances estimated from the scan use the long pulse data and therefore will underestimate the actual conductance as discussed in Section 5. Direct comparisons can be made with the two data sets in Figure 14(a) because only particle precipitation is the major contributor to the conductance. Morphologically, the two data sets respond equally to the enhancement in conductance near 74.6° and are relatively in agreement poleward of this feature. The Pedersen conductances near 74.6° compare well while the radar estimate of the Hall conductance is nearly twice as large as the DMSP estimate. Equatorward of this feature and at the latitude near closest approach of 74°, we find significant differences between the two data sets, which can only be attributed to temporal variability.
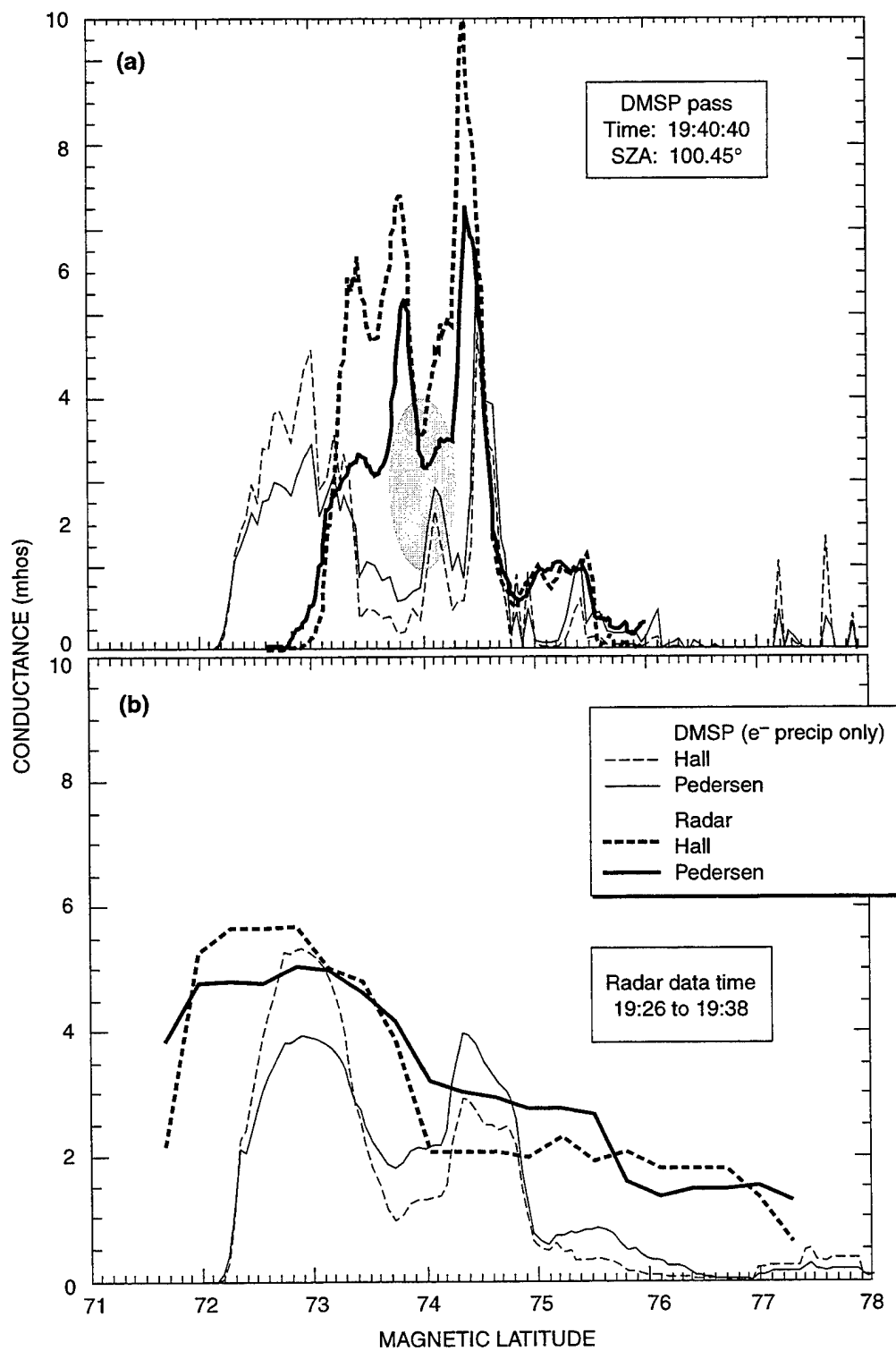
Figure 14(b) compares the smoothed DMSP conductance from the pass with radar estimates of conductance from position measurements taken about 10 minutes prior to the pass. Here we find good comparisons between the two data sets.

6.5 11 February 1996—Day Number 042

A plot of the DMSP/radar azimuth-elevation coverage and the magnetic latitude–time coverage for this day were presented in Figure 2. Again, the World Day antenna mode is used. The closest coincidence between the two measurements occurs near 73.5° magnetic latitude during a dwell measurement with less than a 2-minute difference between measurements covering the 72.5 through 75° magnetic latitudes. The solar zenith angle for this pass was about 91° at 125 km altitude.

The Pedersen and Hall conductances from the single cycle of radar position measurements taken during the time of the DMSP pass are compared with the DMSP conductance estimates in Figure 15. Between 72 and 74° magnetic latitude the radar-derived conductances compare very well with DMSP conductance estimates. The radar measurements may have been subject to some temporal variability as the two elevation scans before and after the dwell data (separated by 15 minutes) show the E region enhancements moved from directly overhead to the south over this time. Disagreement at higher latitudes could also be due to temporal variability between data sets. The discrepancy in the two measurements between 74 and 75.5°, particularly in the Pedersen conductance, is most likely due to the sun's twilight position illuminating the upper E region and F region, which contributes about 1 mho to the Pedersen and Hall conductance.

The data taken near closest coincidence are circled in Figure 15. Here, we find reasonable agreement in both estimates of Hall and Pedersen conductance.

36

(a)

DMSP pass
Time: 19:40:40
SZA: 100.45°

(b)

DMSP (e⁻ precip only)
- - - - - Hall
——— Pedersen

Radar
▪▪▪▪▪ Hall
━━━ Pedersen

Radar data time
19:26 to 19:38

CONDUCTANCE (mhos)

MAGNETIC LATITUDE

6536fr/f14

Figure 14   DMSP / RADAR CONDUCTANCE COMPARISONS: 8 JANUARY 1996
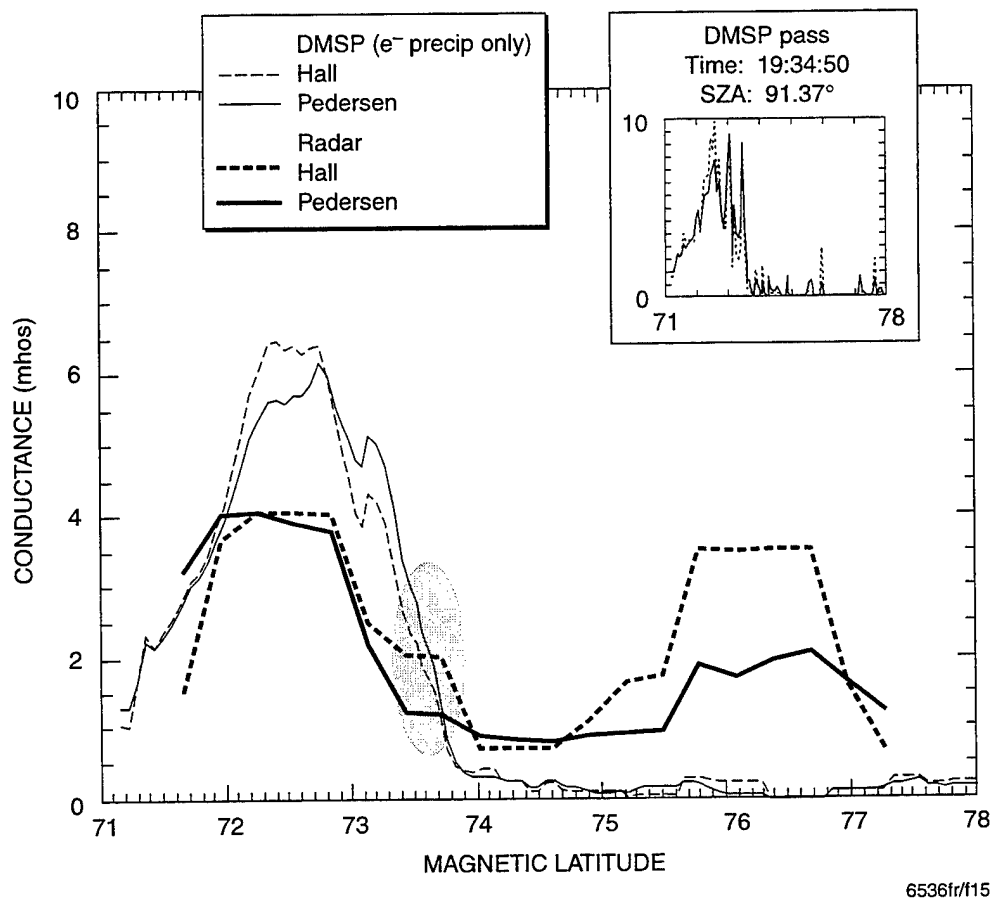
37

Figure 15 DMSP / RADAR CONDUCTANCE COMPARISONS: 11 FEBRUARY 1996

6536fr/f15

6.6 19 February 1996—Day Number 050

A plot of the DMSP/radar azimuth-elevation coverage and the magnetic latitude-time coverage for this day are presented together in Figure 16. Again, the World Day antenna mode is used. The time interval used in Figure 16(b) is less than previous plots and shows the closest coincidence between the two measurements occurs near 73.5° magnetic latitude during a dwell measurement. The solar zenith angle for this day is again close to 90° at 125 km altitude.
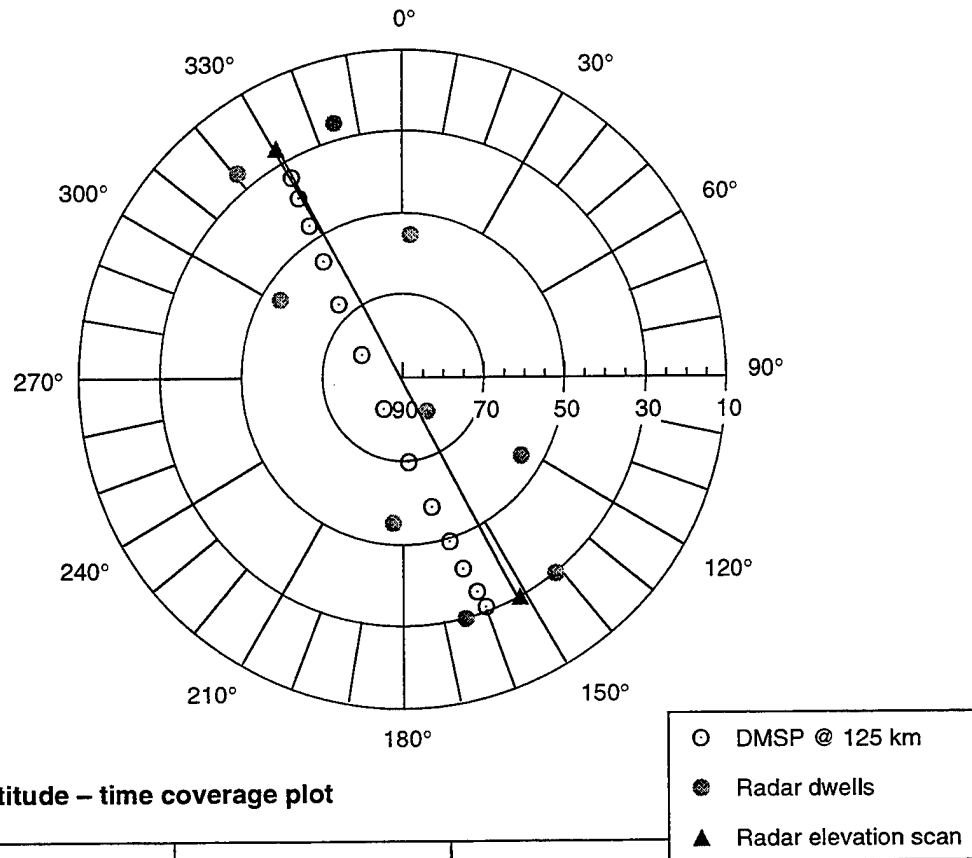
The Pedersen and Hall conductances from the single cycle of radar position measurements taken during the time of the DMSP pass are compared with the DMSP conductance estimates in Figure 17. Here we find rather overall poor agreement between the two data sets. By inspection of the elevation scans prior to and after the cycle of position measurements, we find that the conditions of the E region are changing significantly between scans resulting in the poor comparison particularly between 75 and 76°. Also, the lower spatial resolution of the World Day mode may cause the dwell measurements to actually miss a feature as narrow as that observed by DMSP, as seen in the inset.

Because of the sun's position near the horizon, a baseline conductance of no more than 2 mhos is seen in both the Hall and Pedersen conductance, which is similar to the 11 February data set with nearly the same solar zenith angle. The closest coincidence near 73.5° would indicate that a correction of the DMSP for solar produced ionization of 1.5 mhos would bring the two measurements into agreement.

6.7 Summary of Events

We have presented detailed comparisons for six DMSP/radar experiments. Three of these experiments occurred during solar illuminated conditions near a solar zenith angle of 60°. We have been able to use these cases to evaluate photoionization models. The other three experiments were during twilight and nighttime conditions. These have been used to evaluate the contribution of precipitating electrons to the conductance estimates. Two separate radar modes were used in this study with the summer observations using the DMSP mode while the winter observations used the World Day mode. The DMSP mode sacrifices temporal resolution for spatial resolution, as discussed in Section 4. From the conductance estimates given in Figures 8, 10, and 12, the radar estimates using the DMSP mode showed very little structure as opposed to the DMSP satellite estimates. The differences may be attributed to temporal variations in the precipitating particle event because of the 30 minutes of integration needed by the radar to complete a north–south cycle of measurements versus the less than 2 minutes needed by the DMSP satellite to cover the same distance. In the 16 July 1996 case, the precipitation detected by the DMSP satellite appeared to have moved through all magnetic latitudes covered by the radar as the radar estimates for conductance, shown in Figure 10(b), were elevated over solar produced estimates but remained relatively flat through all magnetic latitudes.

39

a. Azimuth – elevation coverage plot

b. Magnetic latitude – time coverage plot
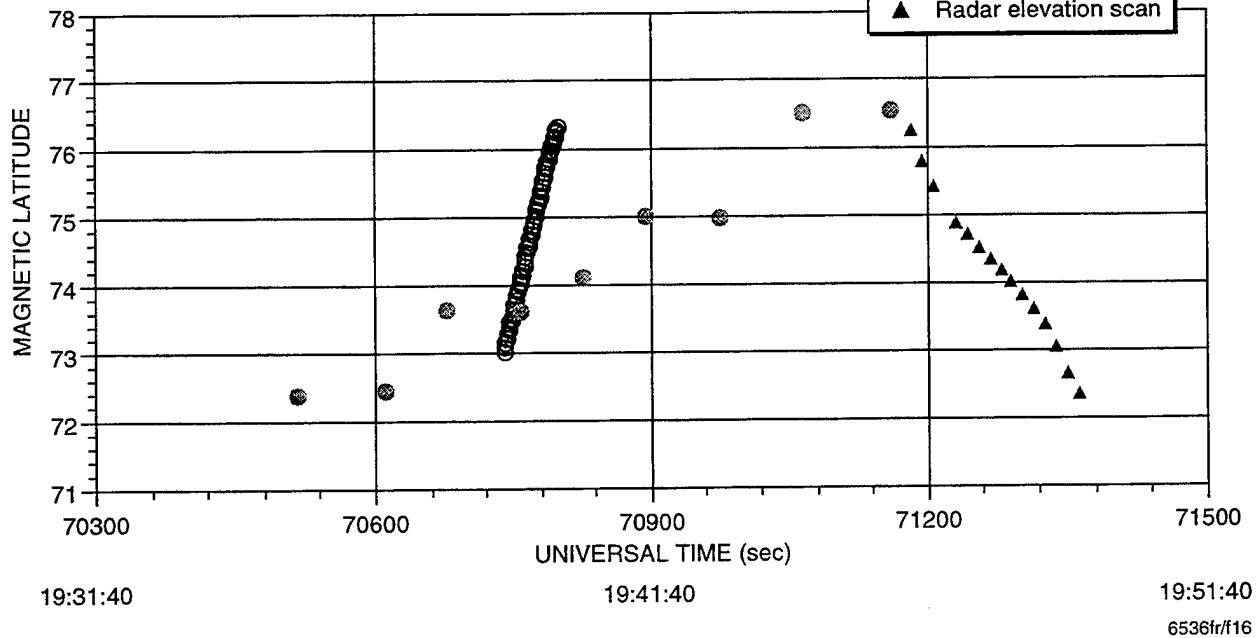

⊙	DMSP @ 125 km
◉	Radar dwells
▲	Radar elevation scan

19:31:40   19:41:40   19:51:40

6536fr/f16

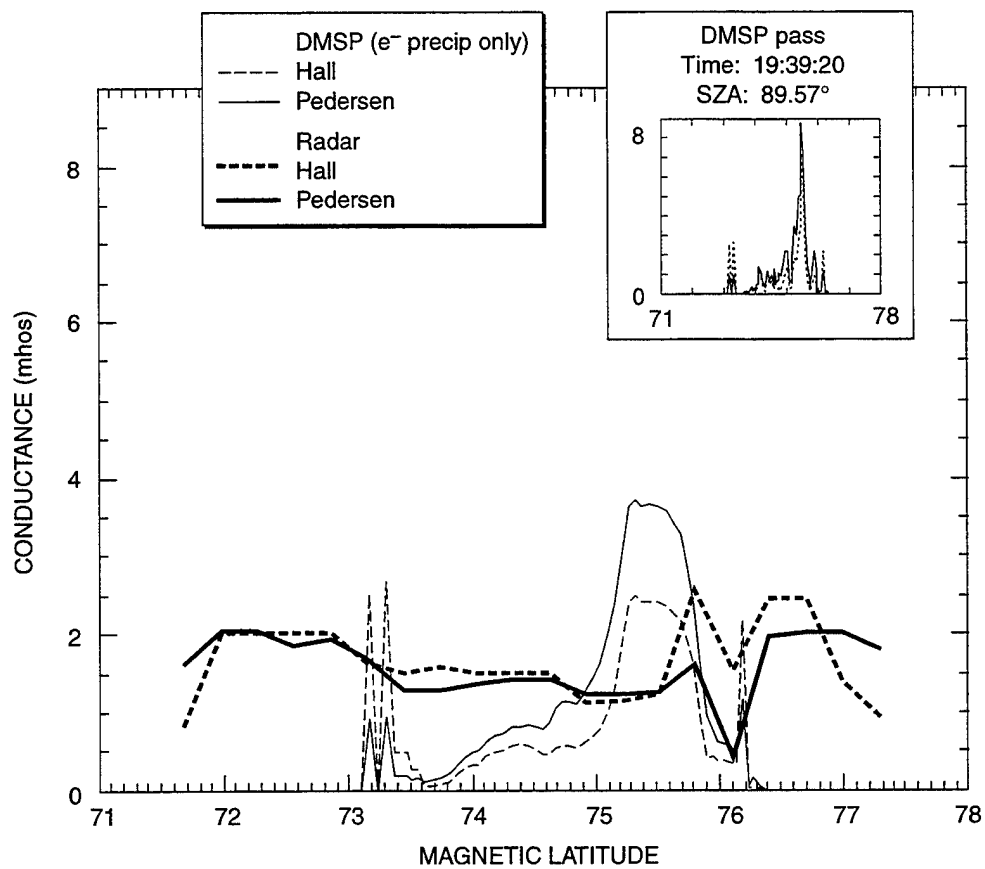**Figure 16   DMSP / RADAR EXPERIMENT: 19 FEBRUARY 1995**

40

Figure 17   DMSP/RADAR CONDUCTANCE COMPARISONS: 19 FEBRUARY 1996

6536fr/f17

41

The World Day mode used in the winter data improved the temporal resolution and better comparisons were achieved between the radar and DMSP estimates of conductance. It, however, is still apparent (see Figure 14(a) for example), that temporal variations in auroral precipitation of less than a few minutes makes it difficult for direct comparisons between the two techniques.

7 CONCLUSIONS

The Defense Meteorological Satellite Program has demonstrated that the Joule heating rate in the high-latitude ionosphere can be estimated from spacecraft. These estimates of the Joule heating rate are subject to a number of assumptions that require validation. Independent ground observations of the same heating process have, therefore, been employed to test the validity of some of these assumptions. The NSF incoherent-scatter radar located at Sondrestrom, Greenland, can measure the plasma parameters of interest and is at a latitude well suited for coincident measurements with DMSP. We have built on the results from the previous DMSP/radar study by Watermann and de la Beaujardiére [1990] with improved techniques to determine the conductance and the Joule heating rate from the Sondrestrom radar. We performed 39 radar experiments dedicated to DMSP overpasses. As in the Watermann and de la Beaujardiére [1990] study, it proved difficult to find experiments that provided active, yet temporally stable, conditions during the brief time of DMSP/radar overlap. We did identify six experiments that permitted direct comparison of the conductance estimates and we used other independent radar measurements to validate the assumptions used in the DMSP analysis of the Joule heating rate. Direct comparison of the radar estimate of the Joule heating rate with DMSP has been deferred for future evaluation when the DMSP Joule heating rate estimates become available.

From our analysis, we have reached a number of conclusions:

- From radar measurements of the Joule heating rate with and without neutral winds we have found that, in general, the estimate of the Joule heating rate using an estimate of the conductance and electric field, our equation (3), is a good proxy. DMSP electric field measurements and Pedersen conductance estimates can, therefore, be useful identifiers of Joule heating events. However, at times of significant directional changes in the electric field and following substorm activity, the neutral winds can be a significant contributor to the Joule heating rate. During times of significant directional changes in the electric field, the neutral winds served to enhance the Joule heating rate by more than 200%. When the electric field direction remained steady for a number of hours, the neutral winds served to reduce the Joule heating rate by about 50%.

- It is important to stress that the neutral winds contribution to the Joule heating rate is dependent on height and weighted by the local Pedersen conductivity. This leads to an inherent problem with the DMSP analysis of the Joule heating rate using equation (1). In

42

(1) it is assumed that the ionosphere is a flat plate and that the height-integrated Pedersen current and the Pedersen conductance can be evaluated separately and then combined to calculate the height-integrated Joule heating rate. This can be a problem if the height profile of the Pedersen current does not match the Pedersen conductivity height profile. This occurs when neutral winds are of importance resulting in a systematic uncertainty in estimating the Joule heating rate in this manner. Thus, even though the DMSP approach using equation (1) purports to include neutral wind effects through the direct measure of the height-integrated current density, the estimate of the height-integrated Joule heating rate is still somewhat ambiguous because of the independent height-integration approach.

- The improved ability to make high-resolution measurements of the E-region by the radar has led to a better estimate of the local conductivity than ever before. We have elucidated the impact of using a long pulse scheme to derive conductance, as was performed by Watermann and de la Beaujardiére [1990], and found it led to systematic errors in estimating the Hall, Pedersen, and Hall-to-Pedersen ratio which may have influenced their conclusions. The magnitude of the error grows as the precipitating particles become more energetic.

- Direct comparisons of radar and DMSP estimates of Pedersen and Hall conductance, ignoring temporal features, were satisfactory during two of the three active precipitating events once appropriate smoothing was applied to the DMSP data to match the resolution of the radar measurement.

- From the daytime experiments it was found that the photoionization models for solar zenith angles near 60° showed good agreement in Pedersen conductance with the Robinson and Vondrak [1984] model while the Hall conductance proved to be consistently overestimated by Robinson and Vondrak [1984] by 30%. In the case of the Hall conductance, the Vickrey et al. [1981] model showed better agreement. This differs from the Watermann et al. [1990] conclusions and could be partly due to pulse smearing effects included in their analysis.

8 RECOMMENDATIONS

The following is a list of recommendations that would help to validate and refine further the methods used to estimate conductance and Joule heating from DMSP data:

- It is apparent from this study and the previous F7 study that simultaneous observations during active ionospheric conditions are difficult. In addition, when active conditions are met, temporal variability of the ionosphere of the order of minutes limits the ability to make a one-to-one correspondence between data sets. This was seen on a number of occasions within this study and past studies. Therefore, our recommendation is to move away from the coincident data sets and take a more statistical approach to the problem. For example, given the fixed local time coverage of the DMSP F12 and F13 satellites and the limited

43

latitudinal coverage of the radar, a collection of independent radar and satellite measurements for these local times and latitudes under certain geophysical conditions can be compared to test the overall accuracy in estimating the Joule heating rate.

- We have also shown in this study that radar measurements can be used to test general assumptions without the need for direct comparison. This is true for the Joule heating rate and the conductances. Further work is needed to ameliorate the role neutral winds play in the DMSP calculation of the Joule heating rate.

- Continued validation of the photoionization models for estimating Pedersen and Hall conductance during daytime passes is required for a wide range of solar zenith angles. This is particularly true for the Hall conductance as we have found that Robinson and Vondrak [1984] overestimate the observed Hall conductance at 60° solar zenith angle by 30% in this study.

Our present and past involvement in DMSP studies with the radar and the recent improvements in the radar's capabilities, makes for a natural progression to future collaboration not considered in this present study.

- Electric Field Measurements—The ability to estimate the electric field from DMSP measurements of the magnetic field and particle data is of particular interest because of the low atomic oxygen densities associated with solar minimum, and the future potential of moving the DMSP orbit to above 1100 km where densities may again limit the measuring capabilities of the drift meter and retarding potential analyzer. The incoherent-scatter radar at Sondrestrom routinely measures the electric field over the invariant latitude band of 82 to 68°. The radar is fully capable of making this measurement during solar minimum conditions. A program to develop this area further would be beneficial to the DMSP program.

- Poynting Flux—A research topic that we have been directly involved in and that is becoming of interest to modelers of magnetosphere–ionosphere (M–I) coupling and satellite experimenters has been the concept of the DC Poynting flux. This concept involves applying the steady state form of Poynting's theorem to the high-latitude ionosphere and evaluating the electromagnetic energy transfer in the M–I system. Based on this concept, the total electromagnetic energy flux into or out of the ionosphere has been evaluated observationally by satellite measurements (HILAT and DE-2) of the dc component of the field-aligned Poynting flux. We have been involved in each of these satellite studies and are well aware of the assumptions inherent to the calculation. For steady state conditions, the field-aligned Poynting flux is equal to the volume-integrated electromagnetic energy transfer rate (J•E) that determines the rate of electromagnetic energy converted, dissipated, or generated within the entire vertical column of the ionosphere. However, a measure of the field-aligned Poynting flux from satellite does not determine how this energy is distributed within the ionosphere. Thayer and Vickrey [1992] illustrated that a measure of the dc field-

aligned Poynting flux is equivalent to determining the Joule heating rate and the mechanical energy transfer rate throughout the entire ionospheric vertical column. Modeling studies by Thayer et al. [1995] and Lu et al. [1995], have shown that the Joule heating rate accounts for more than 70% of the electromagnetic energy converted in the ionosphere with the conductivity-weighted neutral wind contributing significantly to the Joule heating rate. We are beginning to test these models by determining the transfer of electromagnetic energy in the ionosphere through direct measurements by the incoherent scatter radar. The DMSP satellite is an excellent platform for determining the field-aligned Poynting flux and, in conjunction with the radar, we can finally evaluate the energy transfer into the ionosphere and how that energy is distributed throughout the ionospheric column. This concept is fundamental in the development of M–I coupling and important to the DMSP program.

9 REFERENCES

Banks, P. M., "Observations of Joule and Particle Heating in the Auroral Zone," *Journal of Atmospheric and Terrestrial Physics,* Vol. 39, pp. 179-193, 1977.

Brekke, A., and C. L. Rino, "High-Resolution Altitude Profiles of the Auroral Zone Energy Dissipation due to Ionospheric Currents," *J. Geophys. Res., 83,* A6, 2517-2524, 1978.

de la Beaujardiére, O., R. Johnson, and V. B. Wickwar, "Ground-Based Measurements of Joule Heating Rates," *Auroral Physics,* pp. 439-448, 1991.

Lu, G., A. D. Richmond, B. A. Emery, and R. G. Roble, "Magnetosphere-Ionosphere-Thermosphere Coupling: Effect of Neutral Winds on Energy Transfer and Field-Aligned Current", *Journal of Geophysical Research,* Vol. 100, No. A10, pp. 19,643-19,659, 1995.

Rich, F. J., M. S. Gussenhoven, and M. E. Greenspan, "Using Simultaneous Particle and Field Observations on a Low Altitude Satellite to Estimate Joule Heat Energy Flow Into the High Latitude Ionosphere," *Annales Geophysicae,* pp. 527-534, 1987.

Rich, F. J., M. S. Gussenhoven, D. A. Hardy, and E. Holeman, "Average Height-Integrated Joule Heating Rates and Magnetic Deflection Vectors Due to Field-Aligned Currents During Sunspot Minimum," *Journal of Atmospheric and Terrestrial Physics,* Vol. 53, No. 3/4, pp. 293-308, 1991.

Robinson, R. M., and R. R. Vondrak, "Measurements of E Region Ionization and Conductivity Produced by Solar Illumination at High Latitudes," *Journal of Geophysical Research,* Vol. 89, No. A6, pp. 3951-3956, 1984.

Robinson, R. M., R. R. Vondrak, K. Miller, T. Dabbs, and D. Hardy, "On Calculating Ionospheric Conductances From the Flux and Energy of Precipitating Electrons," *Journal of Geophysical Research*, Vol. 92, No. A3, pp. 2565-2569, 1987.

Thayer, J.P., and J.F. Vickrey, "On the Contribution of the Thermospheric Neutral Wind to High Latitude Energetics," *Geophysical Research Letters*, Vol. 19, No. 3, pp. 265-268, 1992.

Thayer, J.P., J.F. Vickrey, R.A. Heelis, and J.B. Gary, "Interpretation and Modeling of the High-Latitude Electromagnetic Energy Flux," *Journal of Geophysical Research*, Vol. 100, No. A10, pp. 19,715-19,728, 1995.

Vickrey, J. F., R. R. Vondrak, and S. J. Matthews, "The Diurnal and Latitudinal Variation of Auroral Zone Ionospheric Conductivity, *Journal of Geophysical Research*, Vol. 86, No. A1, pp. 65-75, 1981.

Vickrey, J. F., R. R. Vondrak, and S. J. Matthews, "Energy Deposition by Precipitating Particles and Joule Dissipation in the Auroral Ionosphere," *Journal of Geophysical Research*, Vol. 87, pp. 5184-5196, 1982.

Watermann, J., and O. de la Beaujardiére, "Joule Heating Investigations Using the Sondrestrom Radar and DMSP Satellites," Technical Report GL-TR-90-0172, Phillips Laboratory Hanscom AFB, Bedford, Massachusetts, USA, June 1990.

Watermann, J., O. de la Beaujardiére, and F. J. Rich, "Comparison of Ionospheric Electrical Conductances Inferred from Coincident Radar and Spacecraft Measurements and Photoionization Models", *Journal of Atmospheric and Terrestrial Physics*, Vol. 55, No. 11/12, pp. 1513-1520, 1993.